


## $^{40}\text{Ar}/^{39}\text{Ar}$ ages and zircon petrochronology for the rear arc of the Izu-Bonin-Marianas intra-oceanic subduction zone

Axel K. Schmitt, Kevin Konrad, Graham D. M. Andrews, Kenji Horie, Sarah R. Brown, Anthony A. P. Koppers, Mark Pecha, Cathy J. Busby & Yoshihiko Tamura

To cite this article: Axel K. Schmitt, Kevin Konrad, Graham D. M. Andrews, Kenji Horie, Sarah R. Brown, Anthony A. P. Koppers, Mark Pecha, Cathy J. Busby & Yoshihiko Tamura (2017):  $^{40}\text{Ar}/^{39}\text{Ar}$  ages and zircon petrochronology for the rear arc of the Izu-Bonin-Marianas intra-oceanic subduction zone, International Geology Review, DOI: [10.1080/00206814.2017.1363675](https://doi.org/10.1080/00206814.2017.1363675)

To link to this article: <http://dx.doi.org/10.1080/00206814.2017.1363675>

 View supplementary material 

 Published online: 06 Sep 2017.

 Submit your article to this journal 

 View related articles 

 View Crossmark data 

ARTICLE



## $^{40}\text{Ar}/^{39}\text{Ar}$ ages and zircon petrochronology for the rear arc of the Izu-Bonin-Marianas intra-oceanic subduction zone

Axel K. Schmitt<sup>a</sup>, Kevin Konrad<sup>b</sup>, Graham D. M. Andrews<sup>c</sup>, Kenji Horie<sup>d,e</sup>, Sarah R. Brown<sup>c</sup>, Anthony A. P. Koppers<sup>b</sup>, Mark Pecha<sup>f</sup>, Cathy J. Busby<sup>g</sup> and Yoshihiko Tamura<sup>h</sup>

<sup>a</sup>Institute of Earth Sciences, Heidelberg University, Heidelberg, Germany; <sup>b</sup>College of Earth, Ocean, and Atmospheric Sciences, Oregon State University, Corvallis, OR, USA; <sup>c</sup>Department of Geology & Geography, West Virginia University, Morgantown, WV, USA; <sup>d</sup>National Institute of Polar Research, Tachikawa, Japan; <sup>e</sup>Department of Polar Science, The Graduate University for Advanced Studies (SOKENDAI), Kanagawa, Japan; <sup>f</sup>Department of Geosciences, The University of Arizona, Tucson, AZ, USA; <sup>g</sup>Earth and Physical Sciences, University of California Davis, Davis, CA, USA; <sup>h</sup>Research and Development Center for Ocean Drilling Science/Mantle and Continental Crust Drilling Research Group, Japan Agency for Marine-Earth Science and Technology (JAMSTEC), Yokosuka, Japan

### ABSTRACT

Long-lived intra-oceanic arcs of Izu-Bonin-Marianas (IBM)-type are built on thick, granodioritic crust formed in the absence of pre-existing continental crust. International Ocean Discovery Program Expedition 350, Site U1437, explored the IBM rear arc to better understand continental crust formation in arcs. Detailed petrochronological (U–Pb geochronology combined with trace elements, oxygen and hafnium isotopes) characterizations of zircon from Site U1437 were carried out, taking care to exclude potential contaminants by (1) comparison of zircon ages with ship-board palaeomagnetic and biostratigraphic ages and  $^{40}\text{Ar}/^{39}\text{Ar}$  geochronology, (2) analysing zircon from drill muds for comparison, (3) selectively carrying out *in situ* analysis in petrographic thin sections, and (4) minimizing potential laboratory contamination through using pristine equipment during mineral separation. The youngest zircon ages in Site U1437 are consistent with  $^{40}\text{Ar}/^{39}\text{Ar}$  and shipboard ages to a depth of ~1390 m below sea floor (mbsf) where Igneous Unit Ig 1 yielded an  $^{40}\text{Ar}/^{39}\text{Ar}$  age of  $12.9 \pm 0.3$  Ma (all errors  $2\sigma$ ). One single zircon (age  $15.4 \pm 1.0$  Ma) was recovered from the deepest lithostratigraphic unit drilled, Unit VII (1459.80–1806.5 mbsf). Site U1437 zircon trace element compositions are distinct from those of oceanic and continental arc environments and differ from those generated in thick oceanic crust (Iceland-type) where low- $\delta^{18}\text{O}$  evolved melts are produced via re-melting of hydrothermally altered mafic rocks. Ti-in-zircon model temperatures are lower than for mid-ocean ridge rocks, in agreement with low zircon saturation temperatures, suggestive of low-temperature, hydrous melt sources. Zircon oxygen ( $\delta^{18}\text{O} = 3.3\text{--}6.0\text{‰}$ ) and hafnium ( $\epsilon\text{Hf} = +10\text{--}+16$ ) isotopic compositions indicate asthenospheric mantle sources. Trace element and isotopic differences between zircon from Site U1437 rear-arc rocks and the Hadean detrital zircon population suggest that preserved Hadean zircon crystals were probably generated in an environment different from modern oceanic convergent margins underlain by depleted mantle.

### ARTICLE HISTORY

Received 25 March 2017  
Accepted 1 August 2017

### KEYWORDS


Zircon; Island Arc; continental crust; geochronology

### Introduction

Expedition 350 of the International Ocean Discovery Program (IODP) had the goal to, for the first time, drill in the rear arc of an archetypical intra-oceanic subduction zone, the Izu section of the Izu-Bonin-Marianas (IBM) intra-oceanic arc (Figure 1). Drilling operations at Site U1437 in the Izu rear arc recovered core down to 1806.5 m below sea floor (mbsf) and penetrated a diverse volcanoclastic succession that provides unique insights into the evolution of the Izu arc. Core from Site U1437 and its zircon cargo significantly contributes to the understanding of across-arc chemical variability in the

production of continental crust, and complements existing studies of along-strike geophysical and chemical variations in an intra-oceanic arc setting (e.g. Tamura *et al.* 2009). The scope of this study is threefold: (1) establishing a radiometric chronostratigraphy for Site U1437 that complements and extends the shipboard age model, which was based on highly successful micropalaeontological and palaeomagnetic data; (2) investigating zircon crystallization from magmatic sources within an intra-oceanic arc in the context of global zircon production; and (3) exploring the trace elemental and isotopic characteristics of intra-oceanic zircon from Site U1437 as a

**CONTACT** Axel K. Schmitt  axel.schmitt@geow.uni-heidelberg.de  Institut für Geowissenschaften, Universität Heidelberg, Im Neuenheimer Feld 234-236, 69120 Heidelberg, Germany

 Supplemental data for this article can be accessed [here](#).

© 2017 Informa UK Limited, trading as Taylor & Francis Group

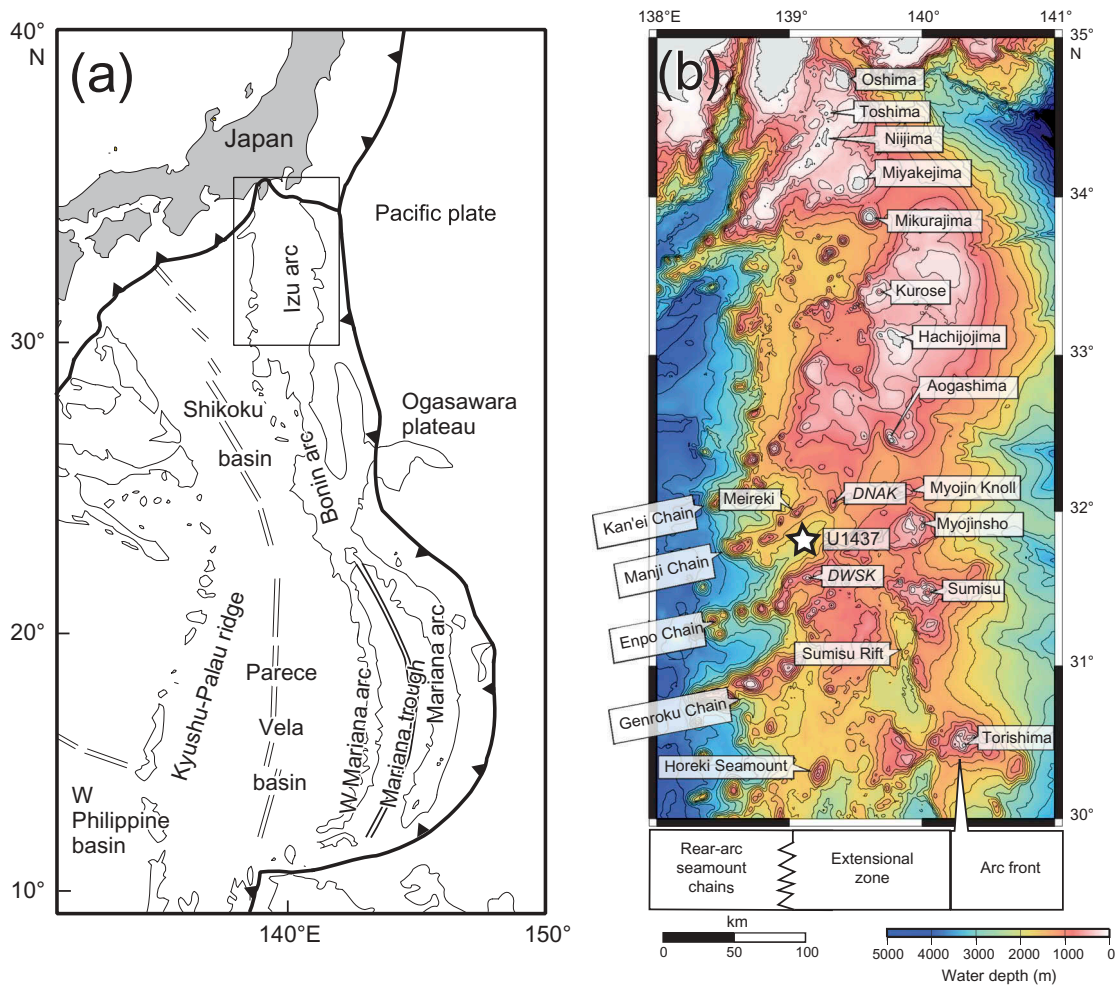


**Figure 1.** Overview map of the relevant section of the Izu-Bonin-Marianas arc showing the location of International Ocean Discovery Program (IODP) Expedition 350, Site U1437. DNAK: Daigo-Nishi-Aogashima Knoll; DWSK: Daisan West Sumisu Knoll. After: Tamura *et al.* (2015).

potential analogue for the Hadean detrital zircon record, which may represent the earliest evidence for the existence of continental crustal on Earth (Harrison 2009; Reimink *et al.* 2014; Kenny *et al.* 2016).

In the course of this study it was also realized that IODP operations have been using drill mud from continental sources in the USA, which also contains abundant zircon. This necessitated the analysis of zircon from drill mud to discriminate Izu rear-arc zircon from potential contamination. Results for sepiolite drill-mud have been published elsewhere (Andrews *et al.* 2016); here, we include new data for zircon in attapulgite drill-mud because both were used during the drilling at Site U1437.

## IODP expedition 350 Site U1437

### Geological background

Site U1437 is located in the central part (between ~30 and 33°N) of the Izu segment of the IBM arc system,

approximately 90 km west of the arc front and 330 km west of the trench (Figure 1). The modern rear arc comprises a series of Neogene seamount chains up to 80 km long that strike nearly perpendicular to the arc front and flank volcano-bounded basins. These are separated from the Neogene to modern arc front by an arc-parallel extensional zone (Figure 1; Taylor 1992; Ishizuka *et al.* 1998; Tamura *et al.* 2015). Drilled Site U1437 is located at 2117 m water depth between the Manji and Enpo seamount chains, referred to as the Mani-Enpo basin (Tamura *et al.* 2015; Busby *et al.* 2017).

Arc magmatism in the region initiated at ca. 52–48 Ma (Arculus *et al.* 2015), and a mature arc crust developed during Eocene to Oligocene time ('Palaeogene arc'; Taylor 1992; Ishizuka *et al.* 2003c, 2006a; Busby *et al.* 2017). Rifting in the rear arc between ca. 25 and 17 Ma created the Shikoku Basin and separated the Eocene to Oligocene rear arc from the arc front, creating the Kyushu-Palau Ridge remnant arc. Spreading in the

Shikoku and Parece Vela back-arc basins likely interrupted magmatism in the arc front, which resumed by ca. 17 Ma and has remained stationary since then (Stern *et al.* 2003). The Neogene Izu arc is inferred to be constructed on Eocene to Oligocene arc crust. The middle crust across the width of the arc has seismic velocities characteristic of felsic to intermediate composition, and varies between 5 and 15 km in thickness along strike (Kodaira *et al.* 2007).

Evolved magmas from the Quaternary arc front fall into three categories (R1–R3; Tamura *et al.* 2009): R1 comprises minor occurrences of rhyolitic differentiates from basalt-dominant volcanoes. These volcanoes are from arc segments with thick middle crust (Tamura *et al.* 2009). R2 erupted from rhyolite-dominant volcanoes (mostly submarine calderas) located over thin middle crust which may have melted to produce abundant rhyolite magma (Tamura *et al.* 2009). A third type of rhyolite (R3) is associated with compositionally bimodal knolls and rift-related lavas in a zone of extension and active rifting immediately west of/behind the arc front (Tamura *et al.* 2009). R3 rhyolites tend to display higher abundances of highly incompatible elements such as K, light rare earth elements (LREE), and Zr (at equivalent  $\text{SiO}_2$ ), compared to rhyolites generated in the arc front volcanoes (Hochstaedter *et al.* 1990; 2000; Tamura *et al.* 2009).

The rear-arc seamount chains (Figure 1) were previously sampled by dredging, and their compositions are dominantly basaltic to andesite with minor amounts of dacite and rhyolite (Hochstaedter *et al.* 2000, 2001; Machida and Ishii 2003; Ishizuka *et al.* 2003a; Machida *et al.* 2008; Tollstrup *et al.* 2010). Eruption ages range between ca. 17 and 3 Ma (Ishizuka *et al.* 1998, 2003c; Hochstaedter *et al.* 2000), and show a younging trend towards the arc front. Magmatic compositions of the rear-arc seamount chains indicate significantly higher abundances of incompatible trace elements (e.g. K, LREE, Zr) compared to the highly depleted arc front magmas (Hochstaedter *et al.* 2000, 2001; Machida and Ishii 2003; Ishizuka *et al.* 2003a; Machida *et al.* 2008; Tollstrup *et al.* 2010). In addition to volcanic samples, plutonic rocks have been recovered on the rear-arc Manji seamount (Ishizuka *et al.* 2002) and from the back-arc Daisan West Sumisu Knoll in the extensional zone at the eastern termination of the Manji seamount chain (Tani *et al.* 2015). These rocks match the calc-alkaline trend and incompatible element enrichment patterns of the volcanic rocks from rear-arc seamount chains. Of particular interest are granodiorites from the Daisan West Sumisu. These compositionally resemble Cordilleran I-type magmas, and yielded zircon whose ca. 8–7 Ma interior ages reveal recycling of pre-existing

Miocene rear-arc crust during a remelting episode at ca. 2.6 Ma indicated by rim ages (Tani *et al.* 2015). Remelting and reprocessing of the mafic arc crust has been related to initiation of extension and rifting behind the arc (Tani *et al.* 2015).

### Drilling results

Drilling at IODP Site U1437 (Figures 1 and 2) generated a record for the Enpo-Manji basin to a depth of 1806.5 mbsf divided into seven lithostratigraphic units (I–VII) and one igneous unit (Ig 1; Tamura *et al.* 2015; Busby *et al.* 2017). Biostratigraphic ages for Site U1437 for the upper 1403 m of the succession (Figure 2) range from lower Pleistocene to upper Miocene; no biostratigraphic ages could be established for depths >1403 mbsf due to low abundance and poor preservation of microfossils (Tamura *et al.* 2015). A detailed magnetostratigraphy downhole to 1302 mbsf (top of Chron C4An, or 8.771 Ma) agrees with the biostratigraphic age model (Figure 2). Only one magnetostratigraphic datum is available from the section at depths >1302 mbsf: Igneous Unit Ig 1 at 1389.35 mbsf displays

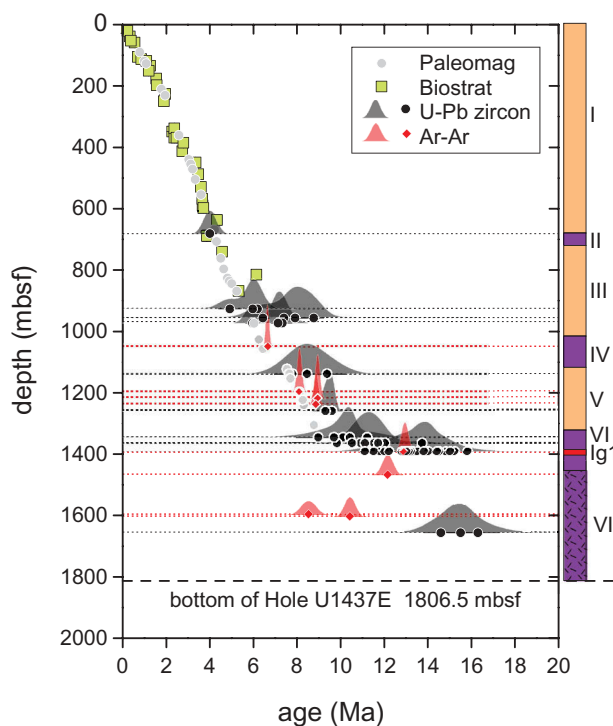


**Figure 2.** Lithostratigraphic units and age model (Tamura *et al.* 2015) with new  $^{40}\text{Ar}/^{39}\text{Ar}$  and U–Pb zircon ages for Site U1437. Units coloured orange on the lithostratigraphic column are dominated by tuffaceous mudstone, while those coloured purple have lapilli tuffs and tuff breccias. The stipple pattern on Unit VII indicates vent-related deposits. Igneous Unit Ig 1 is a rhyolite intrusion with peperite margins (Tamura *et al.* 2015; Busby *et al.* 2017).

reversed polarity, which indicates an age below the older limit of normal Chron C5n.2n at 11.056 Ma (Tamura *et al.* 2015).

Lithostratigraphic Units I–VII (Tamura *et al.* 2015; Busby *et al.* 2017) differ from each other by relative abundance of tuffaceous mudstone, tuff, lapilli-tuff, and tuff-breccia intervals as well as texture and clast composition (where macro- and/or microscopically observable; Figure 2). Units I (0–682.12 mbsf; 0–~4.3 Ma), III (726.50–1017.88 mbsf; ~4.4–6.2 Ma), and V (1120.11–1320.00 mbsf; ~7.5–9 Ma) are dominated by tuffaceous mud or mudstone, which make up ~88%, ~64%, and ~69% of these units, respectively. These fine-grained deposits typically contain significant amounts of glass shards mixed with hemipelagic sediment or material from dilute turbid flow or bottom currents. The remainders of Units I, III, and V comprise ash or tuff whereas deposits with lapilli-sized clasts are rare. Unit II (682.12–726.50 mbsf; ~4.3–4.4 Ma) by contrast has much more lapilli-tuff, pumice lapillistone and tuff (~75%) and lacks tuffaceous mudstone (~25%) compared to Units I or III. The relatively coarse clast size, monomictic composition (dacite), and sedimentary structures suggest that Unit II comprises deposits from subaqueous density currents generated by proximal explosive eruptions. Unit IV (1017.88–1120.11 mbsf; ~6.2–7.5 Ma) has abundant lapilli-tuff and lapillistone intervals and less tuff and tuffaceous mudstone than Units I, III, and V. It resembles unit VI (1320.00–1459.80 mbsf; >9 Ma) because of the presence of thick (up to several metres) of polymictic, mostly evolved, lapilli-tuffs. The coarse-grained, polymictic lapilli-tuffs and lapillistones in Units IV and VI presumably resulted from high-concentration density currents generated by mass wasting or resedimentation from one or more volcanoes, or proximal explosive eruptions.

Igneous Unit Ig 1 (1388.86–1390.07 mbsf) is a hornblende-bearing rhyolite (~74.5% SiO<sub>2</sub>) with sieve-textured plagioclase, large anhedral to subhedral quartz, minor opaques, and accessory zircon. The upper contact of Igneous Unit Ig 1 is chilled and the overlying lapilli tuff is baked, indicating that it is an intrusion rather than a clast or lava. Its lower contact is peperitic, defined as a magma-wet sediment mixture (Busby-Spera and White 1987); the contact shows complex mingling between the intrusion and the host lapilli tuff, including crenulated lobate margins on the intrusion and dispersal of magma into the host on the mesoscopic to microscopic scale (Tamura *et al.* 2015; Busby *et al.* 2017). This indicates that unit VI was water-saturated and unlithified when the rhyolite sill was intruded, i.e. they are penecontemporaneous (Tamura *et al.* 2015; Busby *et al.* 2017).

Unit VII (1459.80–1806.50 mbsf; >10.97–11.85 Ma) differs from all other units by the presence of largely uniform successions of extremely thick-bedded, non-graded, non-stratified, poorly sorted andesite lapilli-tuffs and tuff-breccias, with andesite blocks up to 10s of cm in size. The upper half of Unit VII is a monomict fragmental andesite generated by submarine quenching of lava. The lower half of Unit VII has blocks that show evidence of hot emplacement (e.g. quenched rims, jig-saw fit clasts, and breadcrust or cauliflower structure). Thus, Unit VII is interpreted as near-vent deposits (Tamura *et al.* 2015; Busby *et al.* 2017).

Geochemical analysis of Site U1437 igneous rocks is mostly based on lapilli- and block-sized clasts from Units II, IV, VI, and VII, as well as from Igneous Unit Ig 1 rhyolite sill, whereas the mixed nature of the extremely fine-grained tuffaceous mud/mudstone dominating Units I, III, and V makes geochemical provenance studies more difficult. Preliminary results based on ship-board analysis will be complemented by more detailed on-shore investigations in progress; reconnaissance analyses are reported here for some zircon-bearing intervals (supplementary data 1). The tentative interpretation of these data is that coarse-grained volcanoclastics from Units II and IV show stronger rear-arc affinity compared to fine-grained tuffs from Units I, III, and V, which have a stronger arc front affinity (Tamura *et al.* 2015). Considering geographic locations, ages, and chemical compositions, the Miocene Meireki (3.76 Ma; Ishizuka *et al.* 1998) and Daigo-Nishi-Aogashima Knoll (5.05 Ma; Ishizuka *et al.* 2003b) seamounts are potential sources for lapilli in unit II, whereas Manji seamount rocks share compositional similarities with clast compositions of Unit IV (Tamura *et al.* 2015). Units VI and VII and Igneous Unit Ig 1 are interpreted as vent-related samples that represent rear-arc magmatism prior to extension and rifting. They are compositionally intermediate between arc front rocks and rear-arc samples from the 17–3 Ma seamounts (Tamura *et al.* 2015).

## Sampling and methods

### <sup>40</sup>Ar/<sup>39</sup>Ar geochronology

#### Sample selection and preparation

Coarse-grained lapilli-tuffs, lapillistones, and lava clasts from lithostratigraphic Units I–VII were sought out for <sup>40</sup>Ar/<sup>39</sup>Ar age determinations based on the presence of fresh plagioclase or hornblende as indicated by ship-board microscopy. However, in absence of useable phenocrysts, some fresh holocrystalline groundmass samples were selected. In addition, Igneous Unit Ig 1 was sampled from a coherent interval in the interior of

the sill. First, samples were crushed and sieved to a 180–250  $\mu\text{m}$  size fraction. Grains were then given deionized water baths to remove fine dust particles prior to drying in a 50°C oven. The grains were then subjected to multiple passes through a magnetic separator to concentrate the desired phases. The grains were then sonicated in multiple heated acid baths for 1 h each in sequential 3N HCl, 6N HCl, 1N HNO<sub>3</sub>, and 3N HNO<sub>3</sub> steps with rinsing in between. Plagioclase grains were given an additional 30 min bath in 5% HF. All samples were then sonicated in ultrapure H<sub>2</sub>O for 1 h prior to drying overnight. The processed grains were again sieved prior to being handpicked under a binocular microscope. All efforts were taken to generate a homogenous separate free of alteration. Spinel and fluid inclusions were avoided when preparing plagioclase separates; however, some samples contained an abundance of unavoidable (micro)inclusions. Samples were placed in aluminium packages and loaded into a quartz vial. Fish Canyon tuff sanidine (FCT-2) was used as a flux monitor and was loaded at the base and top of the quartz vial and between every three samples. The vials were then irradiated for 6 h at the Oregon State University (OSU) TRIGA reactor.

### Mass spectrometry

All <sup>40</sup>Ar/<sup>39</sup>Ar age determinations were obtained with OSU's multi-collector ARGUS VI mass spectrometer following the general methods outlined in Balbas *et al.* (2016). Grains were analysed in vacuo using a CO<sub>2</sub> laser with an initial low-power preheating step followed by 17–24 heating steps (with the exception of four preheating steps for the <1 mg amphibole Sample 350-U1437E-19R-1, 126–130 cm). Blanks were analysed at

the start, end, and after every two or three heating steps during each experiment. Each heating step analysis was blank-corrected by fitting a polynomial function to the blanks analysed during the experiment. Air standards and baselines were analysed in batches at least once a day to calibrate mass based discriminations and collector based discriminations respectively. All presented age results were normalized to a FCT-2 age of  $28.201 \pm 0.046$  Ma ( $2\sigma$ ; Kuiper *et al.* 2008) and calculated using the decay constant ( $5.530 \pm 0.097 \times 10^{-10} \text{ a}^{-1}$ ;  $2\sigma$ ) and equations of Min *et al.* (2000). Ages and uncertainties were calculated using ArArCALC (Koppers 2002) with reported uncertainties including ion counting statistics, blank corrections, irradiation constants, J-curve, collector calibrations, mass fractionation, and decay of <sup>37</sup>Ar and <sup>39</sup>Ar for the internal uncertainty and the errors on the branched K decay constant, as well as the FCT-2 sanidine age as an external uncertainty.

### Zircon petrochronology

#### Sample selection and preparation

Sampling for zircon geochronology targeted mostly evolved tuff, evolved lapilli-tuff (or lapillistone), and tuff-breccia intervals, as well as Igneous Unit Ig 1 (Figure 3). Thirty-seven quarter-round core samples (average volume ~100 cm<sup>3</sup>; minimum ~13 cm<sup>3</sup>; maximum 390 cm<sup>3</sup>) from Units I to VII were processed by a Southern California consortium comprising California State University Bakersfield (CSUB) and University of California Los Angeles (UCLA). Igneous Unit Ig 1 was previously sampled by the Southern California consortium for *in situ* analysis using

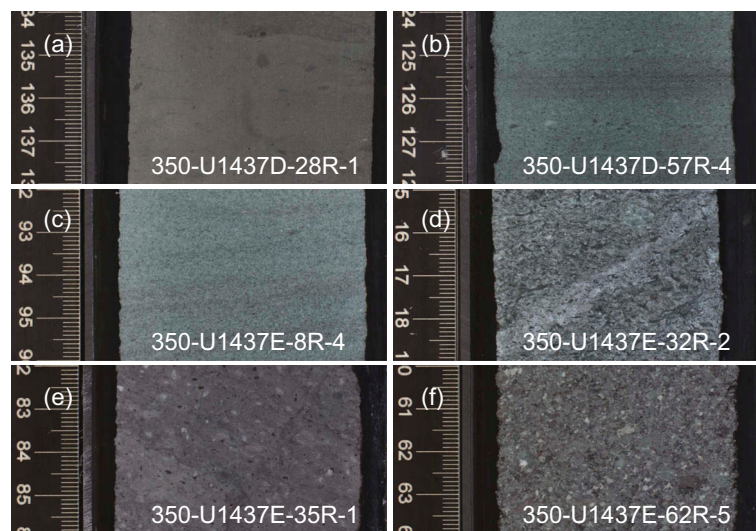


Figure 3. Selected core photographs for zircon-bearing sections of Site U1437.

petrographic thin sections (Tamura *et al.* 2015). In addition, zircon crystals were extracted from attapulgite (FLORIGEL® HY distributed by Active Minerals International), which was used as drill mud at Site U1437 by the JOIDES Resolution Science Operator. A Japanese consortium comprising researchers from the Japan Agency for Marine-Earth Science and Technology (JAMSTEC) and National Institute of Polar Research (NIPR) processed another 39 samples from Units VI–VII and Igneous Unit Ig 1 (sample details in supplementary material).

Procedures of the Southern California consortium started with hand-scrubbing of core samples using a stiff wire-brush and then crushing by hand to gravel-sized pieces (<5 cm in diameter). The gravel was reduced further through a jaw-crusher and a BICO disc mill to a fine sand-sized powder. The powder was processed through a Wilfley water table and the heavy concentrate collected. The concentrate was sieved to <250 µm, passed under an Nd hand magnet to remove magnetite, and then processed through a Frantz LB-1 magnetic separator to remove other magnetic minerals. The non-magnetic fraction was passed through a density separator column filled with methylene iodide (MEI; 3.3 g/cm<sup>3</sup>) to concentrate zircon. Hand-picked zircon crystals were then placed on adhesive tape together with reference zircon AS3 (Paces and Miller 1993), 91500 (Wiedenbeck *et al.* 2004), and 61308A (Wiedenbeck *et al.* 1995) and cast in epoxy (Buehler Epoxycure). After hardening the grains were sectioned by removing approximately one-third of their thickness using SiC (1200 grit) grinding paper and diamond (3 and 1 µm) embedded in mylar film. The final polishing used 0.25 µm diamond paste on hard paper placed on a glass base plate. Mounts were carbon coated for imaging using a TESCAN Vega scanning electron microscope (SEM) equipped with a TESCAN Rainbow cathodoluminescence (CL) detector allowing synchronous acquisition of photoemission in three channels (red, green, and blue). The carbon coat was subsequently removed by gentle polishing using 0.25 µm diamond paste as before, and the mount surfaces were then sputter-coated with Au prior to SIMS analysis. The typical Southern California consortium analysis sequence maximized preservation of the grains by avoiding intermittent sample regrinding/polishing, and progressed via: (1) SIMS oxygen isotope, (2) SIMS U–Pb geochronology, (3) SIMS trace element, and (4) LA-ICP-MS hafnium isotope (at the Laserchron Facility of University of Arizona) analyses.

Samples selected by JAMSTEC and NIPR were disintegrated along grain boundaries by a high-voltage pulse power fragmentation device (SELFRAG Lab).

Samples were immersed in water and fragmented to <760 µm using high-voltage pulses of 120 kV. After rock disintegration, zircon grains were concentrated using conventional mineral separation technique, including heavy liquid separation with methylene iodide and magnetic separation. The external morphologies of the hand-picked zircon grains were imaged by SEM at low vacuum (LV-SEM; JEOL JSM-5900LV at NIPR). Crystals were mounted together with reference zircon TEMORA2 (Black *et al.* 2004) and OD3 (Lukács *et al.* 2015) in epoxy resin (Petropoxy 154, Burnham Petrographics). After curing, epoxy mounts were sectioned at an equatorial plane and polished using diamond (15, 6, 3, and 1 µm). Internal structures were imaged using backscattered electron and CL microscopy using LV-SEM equipped with a Gatan mini CL detector (15 kV accelerating potential and ~0.1 nA beam intensity). Prior to sensitive high-resolution ion microprobe (SHRIMP) analysis, mount surfaces were washed in diluted HCl and rinsed in ultrapure water to remove lead contamination, and then coated with a conductive Au layer. After SHRIMP analyses, the Au coat was removed, and mounts were re-coated with carbon for true colour CL imaging using a Gatan ChromaCL2 installed on a field emission SEM (FE-SEM; JEOL JSM-7100F) at NIPR (5 kV/3 nA). Some regrinding/sectioning was required to remove the <sup>16</sup>O-contaminated craters from SHRIMP analysis at NIPR prior to oxygen isotope analysis by SIMS at Heidelberg University.

Selected host rocks used for zircon extraction were also analysed by X-ray fluorescence (XRF) and inductively coupled plasma mass spectrometry (ICP-MS) methods at the GeoAnalytical Lab of Washington State University. Digestion for XRF and ICP-MS used sample powder fusion with dilithium tetraborate (Li<sub>2</sub>B<sub>4</sub>O<sub>7</sub>) followed by an open-vial mixed acid digestion for solution ICP-MS. XRF analytical methods are described in Johnson *et al.* (1999) and ICP-MS internal standardization in Doherty (1989); data are plotted in Figure 4 and reported in supplementary data 1. Intervals which were processed but failed to yield any zircon are listed as supplementary data 2.

### U–Pb dating

U–Pb zircon geochronology by the Southern California consortium was carried out in three analytical sessions using the CAMECA ims 1270 ion microprobe at UCLA using established protocols for the analysis of late Cenozoic zircon (Schmitt *et al.* 2003). Primary beam intensities for mass-filtered <sup>16</sup>O<sup>−</sup> were ~20 and ~40 nA with a spot size of ~20–30 µm with depths after analysis being approximately one-tenth of the crater diameter.

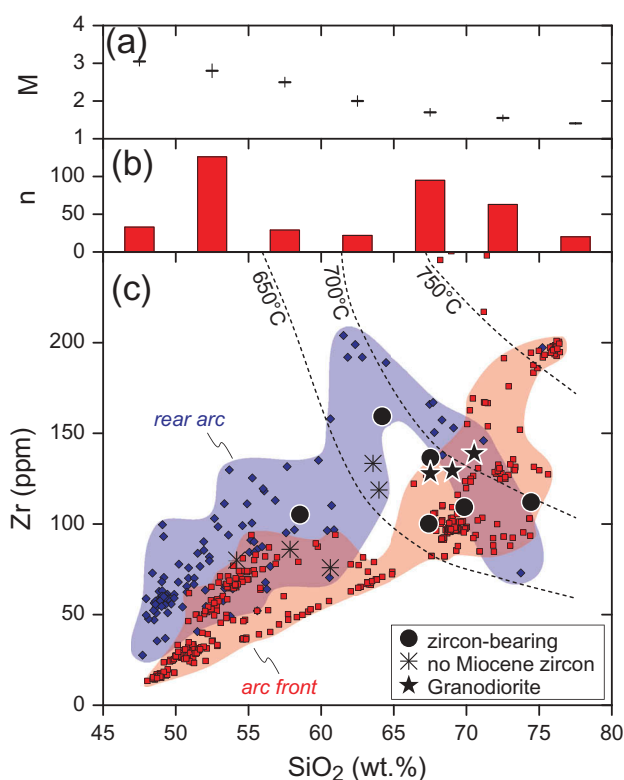


**Figure 4.** Literature and post-expedition (this study) whole rock Zr versus SiO<sub>2</sub> compositions of arc-front and rear-arc igneous rocks. (a) Average and standard deviation for *M*-values calculated from Izu-Bonin arc whole rock data binned in 5 wt.% SiO<sub>2</sub> steps. Histogram (b) indicates the sampling frequency for data bins. (c) Compositions of zircon-bearing and zircon-free samples from Site U1437 in comparison to literature data for volcanic rocks granodiorites from Tani *et al.* (2015). 'No Miocene zircon' are samples from Site U1437 from which zircon was separated with ages significantly older than Miocene; these are likely derived from drill mud and thus irrelevant for zircon saturation. Isotherms are calculated for the average melt compositions (*M*-values) in (a) using the zircon saturation calibration of Boehnke *et al.* (2013). Positive correlations suggest melt evolution under conditions of zircon undersaturation; only rear-arc rocks with SiO<sub>2</sub> > 62 wt.% show a negative correlation for Zr versus SiO<sub>2</sub> suggestive of zircon fractionation. References used: Taylor and Nesbitt (1998), Ishizuka *et al.* (2002, 2006b), Kuritani *et al.* (2003), Machida and Ishii (2003), Yokoyama *et al.* (2003), Tamura *et al.* (2005, 2007, 2009), Shukuno *et al.* (2006), Machida *et al.* (2008), Kimura *et al.* (2010), and Tollstrup *et al.* (2010).

Oxygen flooding was used at the saturation pressure to enhance sensitivity for Pb. A <sup>204</sup>Pb-based common Pb correction was used for reference zircon (except 61308A), whereas <sup>207</sup>Pb was used as a proxy for common Pb for 61308A and unknowns. Reproducibility of <sup>206</sup>Pb\*/<sup>238</sup>U ages for AS3 (1099 Ma; Paces and Miller 1993) used as a primary reference for the UO<sup>+</sup>/U<sup>+</sup> versus U–Pb relative sensitivity calibration was ~2–3% (rel.), and accuracy of the weighted average <sup>206</sup>Pb\*/<sup>238</sup>U

ages based on comparison with replicate analyses (*n* = 10 each) on 91500 and 61308A reference zircon was –1.5% and –2.8% (relative deviation from reported ages of 1065 and 2.488 Ma; Wiedenbeck *et al.* 1995). Th/U in unknown zircon was determined from measured <sup>232</sup>Th<sup>+</sup>/<sup>238</sup>U<sup>+</sup> using a relative sensitivity factor calibrated on measured <sup>208</sup>Pb\*/<sup>206</sup>Pb\* of AS3 reference zircon. Uranium abundances were estimated from U<sup>+</sup>/<sup>94</sup>Zr<sub>2</sub>O<sup>+</sup> in relation to 91500 zircon with 81 ppm U (Wiedenbeck *et al.* 2004).

U–Pb dating by SHRIMP-II at NIPR was carried out based on procedures reported by Horie *et al.* (2013). An O<sub>2</sub><sup>–</sup> primary ion beam of about 2.2 nA was used to sputter zircon from an ~14 μm diameter spot. A retardation lens system was used in the secondary ion column to mitigate the contribution of scattered ions, and the mass spectrometer was adjusted for maximum transmission at a mass resolving power *M*/Δ*M* of ~5300 (at 1% peak height) required to resolve isobaric interferences on Pb isotopes. TEMORA2 (<sup>206</sup>Pb/<sup>238</sup>U age = 416.8 ± 1.3 Ma; Black *et al.* 2004) and 91500 (U concentration 81 ppm; Wiedenbeck *et al.* 2004) were used as reference materials for the calibration of U–Pb as (<sup>206</sup>Pb/<sup>238</sup>U)/(<sup>254</sup>UO/<sup>238</sup>U)<sup>2</sup> and U concentration of zircon, respectively. Data reduction followed Williams (1989) and used the SQUID Excel macro of Ludwig (2008). A correction for common Pb was made on the basis of the measured <sup>204</sup>Pb (for standards) and <sup>207</sup>Pb (for unknowns) using common Pb compositions from the Stacey and Kramers (1975) Pb evolution model calculated using the Isoplot/Ex software (Ludwig 2001). Errors on weighted means of standard measurements were 0.17% (*n* = 122, 1σ) with external spot-to-spot errors of 0.98%. To ensure the accuracy of comparatively young U–Pb ages, OD-3 zircon (32.853 ± 0.016 Ma; Lukács *et al.* 2015) was analysed under the same conditions yielding a weighted average of 32.9 ± 0.2 Ma (*n* = 49).

Corrections for initial <sup>230</sup>Th disequilibrium in Site U1437 zircon (e.g. Wendt and Carl 1985) are minor compared to analytical uncertainties, and consequently data from both participating consortia are presented without this correction. The corrections would add ca. 0.1 Ma to the reported ages (supplementary material).

### Trace element analysis

Trace element in zircon were analysed using CAMECA ims 1270, ims 1280-HR, and SHRIMP-II instruments at UCLA, Heidelberg University, and NIPR, respectively. Two sessions took place at UCLA and one at Heidelberg University. Primary beam intensities of ~12–16 nA <sup>16</sup>O<sup>–</sup> were used with spot sizes smaller than the targeted craters generated by the U–Pb analyses so that trace element and age analysis sampled the same crystal domains. Analytical procedures applied energy filtering



(–100 eV) at low ( $M/\Delta M = 2000$ ) mass resolution and peak-stripping of LREE oxide and hydride interferences with relevant atomic to oxide ratios determined for each session by analysis of doped rare earth element (REE) glasses free of such interferences (Monteleone *et al.* 2007). NIST SRM 610 glass was used as a primary reference to calibrate relative sensitivity factors using  $^{30}\text{Si}^+$  as the normalizing species and major and trace element abundances from (Pearce *et al.* 1997). Matrix effects were mitigated by using high-energy secondary ions, and bias between glass and zircon was determined to be insignificant as indicated by replicate analyses ( $n = 17$ ) of 91500 reference zircon where data for trace elements (Ti, REE, Hf, Th, and U) are within <10% of values reported in Wiedenbeck *et al.* (2004) and Liu *et al.* (2010). The exceptions are La, Pr, and Nd which deviate from the recommended values by +130%, –27%, and –15%, respectively. Given the low abundances and overall scatter of reported values for these elements in 91500 zircon, these deviations are considered insignificant.

Trace element analysis by SHRIMP-II was carried out in two analytical sessions based on procedures reported by Horie *et al.* (2013).  $\text{O}_2^-$  primary ion beam intensity was 1.1 nA with the resulting spot having lateral dimensions of 14  $\mu\text{m}$  in diameter. Mass stations for REE and additional trace elements (Y, Nb, and Hf) were scanned from 89 to 180 at high mass resolution ( $M/\Delta M \sim 10,000$ ) in to resolve isobaric interferences from light REE oxides species onto heavy REE mono-atomic species (e.g. Horie *et al.* 2013). Intensities for the elements of interest are referenced to  $^{96}\text{Zr}^+$  derived from the matrix component of zircon and calibrated against 91500 zircon (Wiedenbeck *et al.* 2004). Analytical procedures for Ti measurements followed those in Horie *et al.* (2013).  $^{30}\text{Si}^+$ ,  $^{91}\text{Zr}^{++}$ , and  $^{49}\text{Ti}^+$  were analysed at a mass resolution  $M/\Delta M$  of  $\sim 4000$  using a similar primary setting as for REE, Y, Nb, and Hf analysis. The average  $^{49}\text{Ti}^+/^{30}\text{Si}^+$  of 10 scans was converted to Ti concentrations by referencing to zircon SL13 (6.3 ppm Ti; Hiess *et al.* 2008). Twenty-three analyses of TEMORA2 yielded Ti concentrations of  $10.2 \pm 2.2$  ppm (1 SD), which is consistent with results in Fu *et al.* (2008) ( $10.2 \pm 7.3$  ppm) within analytical uncertainties.

### Oxygen isotope analysis

Oxygen isotopes in zircon were analysed at UCLA and Heidelberg University using CAMECA ims 1270 and ims 1280-HR ion microprobes, respectively. These analyses were typically carried out prior to geochronology and trace element analysis. The exception was the JAMSTEC/NIPR mount where oxygen isotopes were analysed subsequent to dating and trace element analysis. This

required regrinding/polishing which unfortunately led to loss of some crystals. Care was taken that mount surfaces were flat, and that unknowns and references were mounted within the innermost 1.5 cm of the mount to minimize bias due to geometry effects. A 2–3 nA  $\text{Cs}^+$  primary beam was focussed to 10–15  $\mu\text{m}$  using an aperture-shaped beam at UCLA and a focussed beam rastered over 10  $\mu\text{m}$  at Heidelberg University. Multi-collection with dual Faraday cups followed techniques described in Trail *et al.* (2007). Instrumental mass fractionation was corrected by analysing AS3 and TEMORA 2 reference zircon (AS3  $\delta^{18}\text{O} = +5.34\text{‰}$ ; Trail *et al.* 2007; TEMORA 2  $\delta^{18}\text{O} = +8.2\text{‰}$ ; Ickert *et al.* 2008) bracketing every 5–6 unknowns ( $\delta$  values are relative to Vienna Standard Mean Ocean Water V-SMOW;  $^{18}\text{O}/^{16}\text{O} = 0.0020052$ ; Baertschi 1976). Reproducibility of the reference zircon was 0.2–0.3‰ (1 SD) over the course of individual sessions. Accuracy was tested by replicate analysis of reference zircon 91500 ( $\delta^{18}\text{O} = +9.86\text{‰}$ ; Wiedenbeck *et al.* 2004) mounted proximal to the unknowns. Averages for 91500 calibrated against AS3 were within <0.5‰ of the recommended value; we therefore assign a conservative absolute uncertainty of the  $\delta^{18}\text{O}$  zircon analyses for the unknowns of 0.5‰ (2 $\sigma$ ).

### Hafnium isotope analysis

Hf isotopic analyses were conducted using a Nu Instruments HR multi-collector ICPMS connected to a Photon Machines Analyte G2 excimer laser, following established analytical protocols described in Gehrels and Pecha (2014). Instrument settings were optimized for laser ablation analysis, and in-run analyses of seven different natural zircon standards (Mud Tank, Temora, FC52, R33, Temora, Plesovice, and Sri Lanka) were analysed and monitored every 15–20 unknowns.

Ablation with a laser beam diameter of 40  $\mu\text{m}$  targeted zircon domains directly over the earlier U–Pb analysis craters. All measurements were made in static mode using Faraday collectors equipped with  $3 \times 10^{11} \Omega$  resistors. Each acquisition consisted of one 40-s integration for backgrounds (on peak with laser idle) followed by 60 one-s integrations with the laser firing. A 30 s delay between laser analyses provided adequate time to ensure the previous sample was completely purged from the collector block. The laser was run in constant energy mode at with an output of 7.5 mJ (fluence  $\sim 8 \text{ J/cm}^2$ ) and a pulse rate of 7 Hz. Isotope fractionation ( $\beta$ ) was accounted for by incorporating the method of Woodhead *et al.* (2004) with  $\beta_{\text{Hf}}$  determined from the measured  $^{179}\text{Hf}/^{177}\text{Hf}$ , and  $\beta_{\text{Yb}}$  from the measured  $^{173}\text{Yb}/^{171}\text{Yb}$  (except for very low Yb signals);  $\beta_{\text{Lu}}$  is assumed to be the same as  $\beta_{\text{Yb}}$ ; and an exponential formula is used for fractionation correction. Yb and Lu interferences are corrected by

measurement of  $^{176}\text{Yb}/^{171}\text{Yb}$  and  $^{176}\text{Lu}/^{175}\text{Lu}$  (respectively), as advocated by Woodhead *et al.* (2004). Isotope ratios of  $^{179}\text{Hf}/^{177}\text{Hf} = 0.73250$  (Patchett and Tatsumoto 1981);  $^{173}\text{Yb}/^{171}\text{Yb} = 1.132338$  (Vervoort *et al.* 2004);  $^{176}\text{Yb}/^{171}\text{Yb} = 0.901691$  (Vervoort *et al.* 2004; Amelin and Davis, 2005);  $^{176}\text{Lu}/^{175}\text{Lu} = 0.02653$  (Patchett 1983) were used and all corrections are done line-by-line. Data reduction protocols account for all standards and unknowns analysed during an entire session, and the  $\beta\text{Hf}$  and  $\beta\text{Yb}$  cut-offs were determined by monitoring the average offset of the standards from their known values resulting in a final standard offset of 0.0000001.  $^{176}\text{Hf}/^{177}\text{Hf}$  uncertainty on the standard analyses for the entire session was determined to be 0.000037 ( $2\sigma$ ).

## Results

### $^{40}\text{Ar}/^{39}\text{Ar}$ geochronology

In total, 13 age experiments were attempted with 11 usable results that yielded  $^{40}\text{Ar}/^{39}\text{Ar}$  isochron intercepts within error of atmosphere ( $^{40}\text{Ar}/^{36}\text{Ar} = 295.5$ ). All uncertainties for  $^{40}\text{Ar}/^{39}\text{Ar}$  age determinations are reported with  $2\sigma$  confidence herein; selected spectra are plotted in Figure 5, and all data are shown in the supplementary materials. The mean square of weighted deviants (MSWD) for each plateau were within acceptable limits, varying between 0.25 and 1.6 for all but the plagioclase separate of Sample 350-U1437E-17R-3, 13–16 cm, which yielded an elevated MSWD of 3.4. Plateaus were typically long and contained between 37% and 100% of the released  $^{39}\text{Ar}_K$ . The K/Ca ( $^{39}\text{Ar}_K/^{37}\text{Ar}_{Ca}$ ) were very low (0.001–0.002) for plagioclase recovered from Unit VI and below (>1460 mbsf), which expresses the depleted composition of these rocks.

Basaltic andesite from Unit IV, 350-U1437D-68R-2, 45–49 cm (~1049 mbsf) was analysed providing a continuous well-defined heating spectrum with an age of  $6.63 \pm 0.04$  Ma. From Unit V, Samples 350-U1437E-15R-5, 94–97 cm (~1201 mbsf; plagioclase;  $8.09 \pm 0.12$  Ma), 350-U1437E-17R-3, 13–16 cm (~1216 mbsf; plagioclase;  $8.92 \pm 0.08$  Ma), and 350-U1437E-19R-1, 126–130 cm (~1243 mbsf; amphibole;  $8.86 \pm 0.09$  Ma) produced reliable plateau ages. However, a plagioclase separate from Sample 350-U1437E-19R-1, 126–130 cm, displayed a heating spectrum that continually increased in apparent age towards higher temperature steps, indicating a gradual increase in excess Ar being released. Thus, no reliable age can be inferred. In contrast, the corresponding amphibole separate (<1 mg) contained a concordant plateau with an atmospheric intercept. From Igneous Unit Ig 1 within Unit VI, a hornblende separate of Sample 350-U1437E-35R-1, 133–142 cm (~1390 mbsf) produced a long and well-

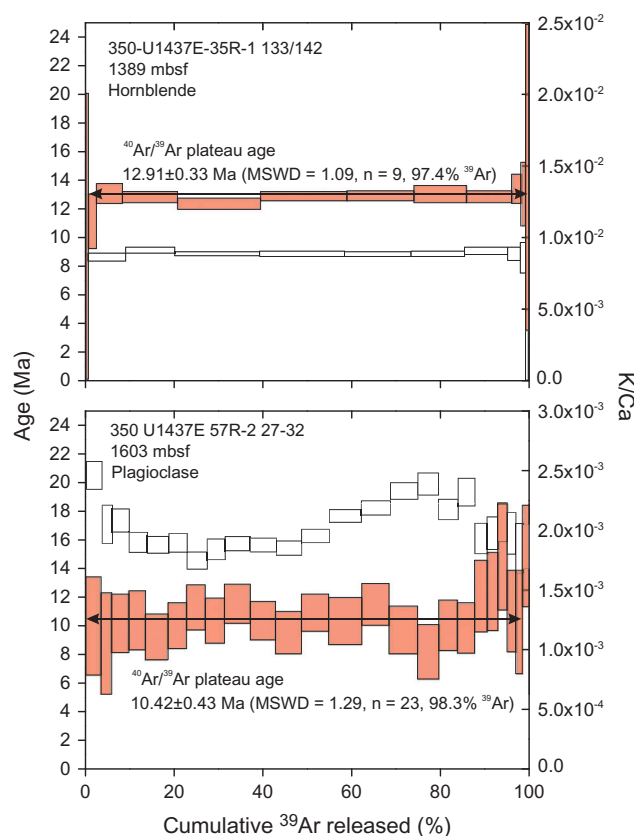


**Figure 5.** Examples for  $^{40}\text{Ar}/^{39}\text{Ar}$  stepwise-heating release spectra and corresponding ages (filled) and K/Ca (open) for (a) hornblende from Sample 350-U1437E-35R-1, 133–142 cm (1389 mbsf) and (b) plagioclase from Sample 350 U1437E 57R-2, 27–32 cm (1603 mbsf). Note order-of-magnitude higher K/Ca in hornblende (a) relative to plagioclase (b). Despite the valid plateau for the plagioclase, the apparent age is too young based on stratigraphic constraints from the overlying intrusive rhyolite which yielded consistent U–Pb zircon and  $^{40}\text{Ar}/^{39}\text{Ar}$  hornblende ages.

defined plateau with an age of  $12.91 \pm 0.16$  Ma. Within unit VII, two splits of plagioclase were analysed from Sample 350-U1437E-43R-2, 105–109 cm (~1468 mbsf) with concordant ages of  $12.15 \pm 0.45$  Ma and  $12.14 \pm 0.38$  Ma (combined age of  $12.15 \pm 0.28$  Ma). Both splits generated reliable age spectra that deviated towards excess Ar patterns (rapid increases in apparent age) at high temperatures. For Sample 350-U1437E-56R-5, 126–130 cm (~1598 mbsf) both a groundmass ( $8.71 \pm 0.12$  Ma) and plagioclase ( $8.54 \pm 0.67$  Ma) separate was produced that was concordant within error generating a combined age of  $8.70 \pm 0.13$  Ma. For Sample 350-U1437E-57R-2, 27–32 cm (~1604 mbsf) a groundmass and plagioclase separate was again attempted with discordant results of  $9.08 \pm 0.10$  Ma and  $10.42 \pm 0.43$  Ma, respectively. The groundmass split contains a slightly elevated isochron intercept of  $303.8 \pm 6.4$  while the plagioclase sample has an atmospheric intercept. A plagioclase

separate was attempted from the deepest portion of the core (Sample 350-U1437E-79R-2, 40–49 cm, ~1798 mbsf), which produced a scattered and unusable plateau, displaying signs of low-temperature apparent age resetting and high-temperature excess Ar.

Overall, the  $^{40}\text{Ar}/^{39}\text{Ar}$  age results are concordant with on-board palaeomagnetic and biostratigraphy constraints (Tamura *et al.* 2015; Musgrave and Kars 2016), as well as U–Pb zircon ages (see below) until the transition to Unit VII, wherein apparent  $^{40}\text{Ar}/^{39}\text{Ar}$  ages become unreasonably young and decrease with depth. This reversal of the age trend also coincides with increasing incompatible element depletion and hydrothermal alteration affecting these units (Tamura *et al.* 2015).  $^{40}\text{Ar}/^{39}\text{Ar}$  ages below Igneous Unit Ig 1 are thus disturbed and unreliable as depositional ages.

### U–Pb zircon geochronology

Zircon at Site U1437 is generally scarce: only 25% and 15% of the intervals processed (by the Southern California and Japanese consortia, respectively) yielded zircon. Even in the zircon-bearing intervals, zircon recovery was mostly low, with one to four extracted crystals per sample (supplementary materials). Exceptions are Samples 350-U1437E-32R-2, 7–29 cm (evolved lapilli-tuff from Unit VI at ~1360 mbsf) and 350-U1437E-35R-1, 83–85 cm (evolved pepritic sill, Igneous Unit Ig 1 at ~1389 mbsf) which yielded 14 and 13 zircon crystals, respectively (Figure 3). The presence of zircon in Igneous Unit Ig 1 was also confirmed by *in situ* analysis of zircon in several petrographic thin sections from Samples 350-U1437E-35R-1, 115–118 cm, and 350-U1437E-35R-2, 42–44 cm. Units II and IV (monomictic, evolved lapilli-tuffs and polymictic, evolved lapilli-tuffs, respectively) completely lacked zircon, despite processing abundant material from multiple intervals. Several intervals in Units III, VI, and VII yielded a few zircon crystals which upon analysis turned out to be unreasonably old (ca. 51 Ma to 1.1 Ga) and thus not part of the Neogene volcanic sequence. We interpret these old zircon crystals as potential drill-mud contaminants based on attapulgite zircon ages ranging from ca. 312 Ma to 1.6 Ga (see below) and sepiolite ages ranging from 1.89 Ma to 2.9 Ga (Andrews *et al.* 2016).

Where Miocene-aged zircon is present, whole-rock Zr abundances are between ~100 and 160 ppm (Figure 4). Zircon saturation model curves using arc front major element compositions to estimate the *M*-value ( $[(\text{Na} + \text{K} + 2 \times \text{Ca})/\text{Si} \times \text{Al}]$  in relation to  $\text{SiO}_2$  (Boehnke *et al.* 2013) imply temperatures of ca. 700°C for zircon to crystallize (Figure 4).

U–Pb zircon ages (supplementary material) are generally homogeneous for individual crystals that were large enough to place spots on core and rim domains (cf. Tani *et al.* 2015). Zircon populations for individual samples, however, often yielded MSWD values near the upper limit for the critical range for a single population (Mahon 1996). The elevated MSWD values are unlikely to be a function of underestimating analytical uncertainties based on the low MSWD of the Quaternary secondary reference zircon 61308A. It is possible, however, that multiple but similar age populations are present in some samples. Where MSWD values exceeded 1, the uncertainties were scaled by the square root of the MSWD to account for excess scatter.

For Units I, III, and V, zircon was extracted mostly from tuffs and tuffaceous mudstone, and one lapilli-tuff. The U–Pb zircon ages between  $4.00 \pm 0.58$  Ma (350-U1437D-28R-1, 127–149 cm, ~681 mbsf) and  $9.46 \pm 0.29$  Ma (350-U1437E-21R-4, 106–108 cm, ~1258 mbsf) closely follow the bio- and magnetostratigraphic age model (Figure 2). Units below ~1258 mbsf are essentially exclusively constrained by radiometric ages. Unit VI contained two lapilli-tuff intervals with zircon present: 350-U1437E-30R-4, 40–42 cm (~1342 mbsf) and 350-U1437E-32R-2, 7–29 cm (~1361 mbsf). U–Pb ages increase in stratigraphic order from  $10.3 \pm 0.4$  Ma to  $11.5 \pm 0.4$  Ma (Figure 2). Igneous Unit Ig 1 occurs within 30 m from the lower sample and yielded a stratigraphically consistent U–Pb zircon age of  $13.9 \pm 0.2$  Ma (350-U1437E-35R-1, 83–85 cm; MSWD = 1.07;  $n = 31$ , Figure 6). This age agrees with a less precise concordia intercept age of  $13.6 + 1.6/-1.7$  Ma from *in situ* analysis of nine small (ca. 20–30  $\mu\text{m}$ ) zircon crystals from Igneous Unit Ig 1 (Tamura *et al.* 2015; Figure 6). It is, however, significantly older than the  $^{40}\text{Ar}/^{39}\text{Ar}$  hornblende plateau age of  $12.91 \pm 0.16$  Ma, suggesting that zircon crystallized prior to emplacement and cooling of Igneous Unit 1. One interval of Unit VII (350-U1437E-62R-5, 60–65 cm, ~1656 mbsf), a polymictic, evolved lapilli-tuff yielded a single zircon which, analysed in triplicate, produced a weighted average U–Pb age of  $15.4 \pm 0.8$  Ma (Figure 2).

### Zircon trace element and isotopic compositions

Neogene zircon from Site U1437 have typically low U abundances (average 120 ppm; range 23–510 ppm). Zircon Th/U averages 0.43 and ranges from 0.24 to 1.0, close to the typical magmatic value (~0.5; Hoskin and Schaltegger 2003). Zr/Hf is higher than chondritic (~36; Anders and Grevesse 1989) with an average of 60, a minimum of 39, and a maximum of 76. Because Zr/Hf in zircon without prior fractionation of zircon is ~72

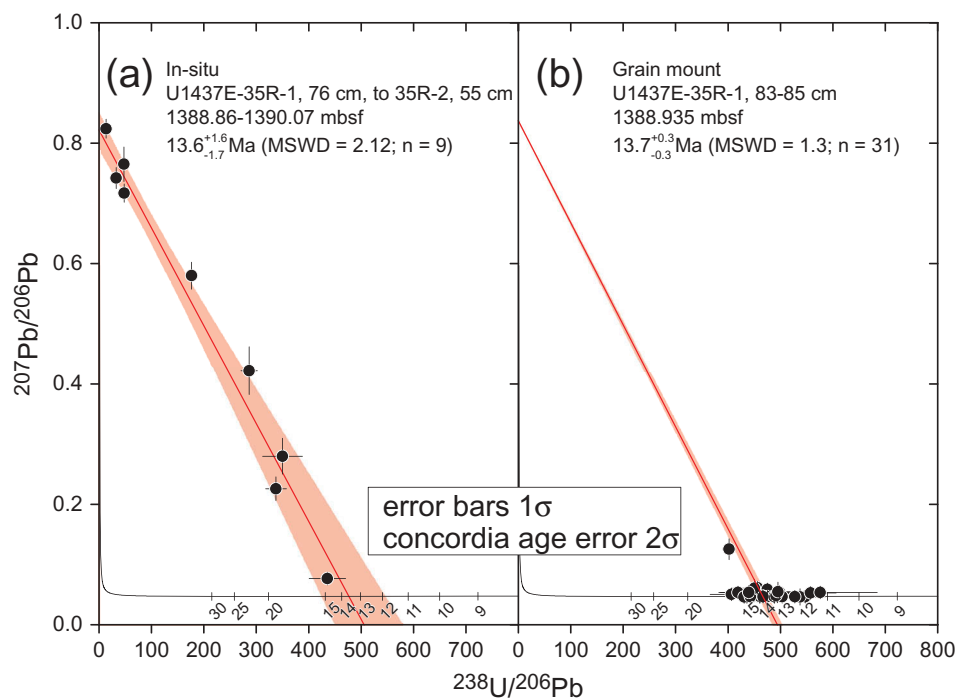


**Figure 6.** *In situ* (a) and crystal separate (b) U–Pb analyses of zircon from Site U1437 Igneous Unit Ig 1.

(calculated from partitioning values in Blundy and Wood 2003), and continuously decreases with zircon fractionation as magma temperatures decrease, the comparatively high Zr/Hf in Site U1437 zircon suggests that zircon crystallized from melts which had barely reached zircon saturation. REE patterns (Figure 7) are characteristic for igneous zircon with strong increases towards heavy REE (HREE) ( $Yb_N/Gd_N = 37\text{--}350$ ; average = 120) and prominent positive Ce anomalies ( $Ce/Ce^* = 1.2\text{--}80$ ; average = 14). Moderately to strongly negative Eu anomalies ( $Eu/Eu^* = 0.07\text{--}0.60$ ; average 0.40) indicate extraction of plagioclase from the melt prior to zircon crystallization. Site U1437 zircon compositions plot in a distinct field in various trace element abundances (Yb, Hf, Hf) and ratio diagrams (e.g. U/Yb, Nb/Yb): they have low Yb, Hf, and Nb/Yb which makes them broadly similar to zircon from oceanic environments (e.g. mid-ocean ridge gabbros and plagiogranites) and distinguishes them from continental arc and oceanic island zircon (Figure 8). Site U1437 zircon, however, has U and U/Yb values that are significantly above those for oceanic zircon (Figure 8). Attapulgitite drill-mud zircon (supplementary data 5), by contrast, closely overlaps with the field for continental arc zircon, as do zircon crystals from sepiolite drill - mud (Andrews *et al.* 2016). Attapulgitite and sepiolite zircon also differ from Site U1437 zircon based on typically higher U (averages attapulgitite = 495 ppm; sepiolite = 345 ppm), lower Zr/Hf (averages attapulgitite = 38; sepiolite = 56),

and more variable but on average lower  $Eu/Eu^*$  (averages attapulgitite = 0.26; sepiolite = 0.32) and  $Yb_N/Gd_N$  (averages attapulgitite = 229; sepiolite = 79).

Ti abundances in Site U1437 zircon are between ~3 and 12 ppm (Figure 9). In igneous rocks where rutile is absent, as is the case for Site U1437,  $TiO_2$  activity ( $a_{TiO_2}$ ) is <1 and Ti-in-zircon thermometry can be systematically biased (Ferry and Watson 2007). By contrast, a silica activity ( $a_{SiO_2}$ ) of 1 is reasonably assumed based on the presence of quartz (e.g. in Igneous Unit Ig 1). For the majority of Site U1437 zircon crystals, the crystallization interval, within reasonable  $a_{TiO_2}$  boundaries from 0.5 to 1 (Ferry and Watson 2007), is therefore between ~800 and 700°C. The slightly higher-temperature range of Ti-in-zircon thermometry, compared to zircon saturation estimates, indicates undersaturation of the melt at  $T > 750^\circ\text{C}$ . High-temperature zircon crystallization could then be due to local oversaturation, e.g. near rapidly crystallizing oxides (Bacon 1989). This agrees with petrographic observations for Igneous Unit Ig 1 where zircon is often enclosed in magnetite.

Oxygen isotopic compositions in Site U1437 zircon average  $\delta^{18}O = 5.1\text{‰}$  with a range from 3.3 to 6.0‰ (Figure 10). Igneous Unit Ig 1 zircon is homogeneous in  $\delta^{18}O$ , with an average of 5.3‰ matching mantle compositions (Valley 2003) and a standard deviation of 0.2‰ ( $n = 20$ ), which is equivalent to the analytical reproducibility. In comparison, attapulgitite and sepiolite zircon has typically more elevated

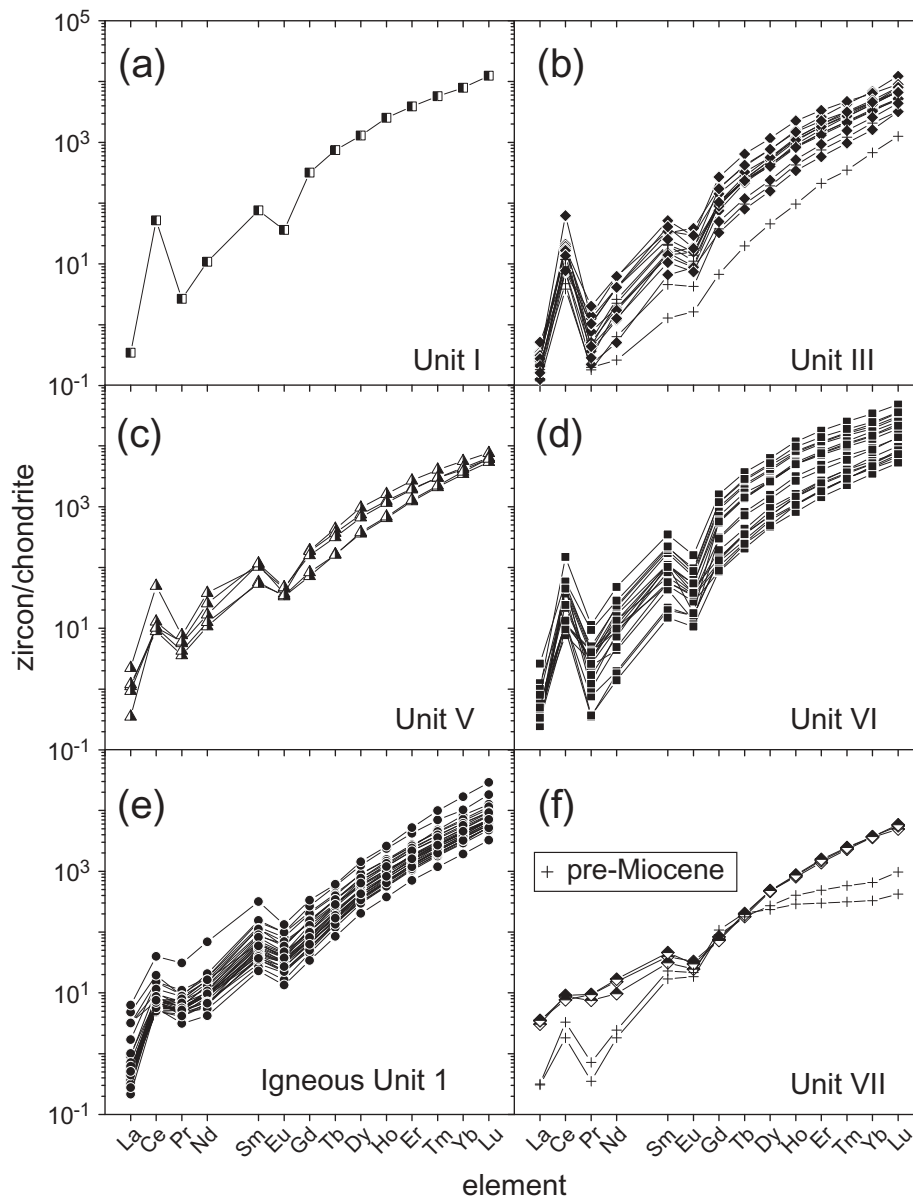


**Figure 7.** Zircon chondrite-normalized rare earth element (REE) patterns for Site U1437. Normalization values from Anders and Grevesse (1989). Pre-Miocene zircon includes potential contaminants from attapulgite and sepiolite drill mud and zircon of unknown provenance.

$\delta^{18}\text{O}$  (average 6.7‰ and range 4.4–10.0‰; average 6.5‰ and range 4.3–9.8‰, respectively).

Hafnium isotopes are highly positive in Site U1437 zircon (present-day value relative to chondritic uniform reservoir (CHUR) value of Bouvier et al., 2008:  $\epsilon\text{Hf}_0 = +10$ – $+17$ ; Figure 10; supplementary material). The range of Hf isotopes in Site U1437 (Figure 10) overlaps with and extends to slightly lower values compared to published basalt-rhyolite whole-rock data for the rear arc and <3 Ma active rift and back-arc knolls ( $\epsilon\text{Hf}_0 = +13$ – $+16$ ; Hochstaedter et al. 2000, 2001; Ishizuka et al. 2002, 2006b; Tollstrup et al. 2010). Rear-arc, active rift, and back-arc knolls tend to have mildly lower  $\epsilon\text{Hf}$  than values

of arc front lavas ( $\epsilon\text{Hf}_0 = +15$ – $+18$ ; Tamura et al. 2007, 2009; Tollstrup et al. 2010). By contrast,  $\epsilon\text{Hf}_0$  is highly negative in attapulgite zircon ( $\epsilon\text{Hf}_0 = -47$  to  $-4$ ; supplementary data 6). This complete lack of overlap implicates Hf isotopes as a useful discriminant for contamination from attapulgite, with the highly positive values in the zircon being consistent with an inter-oceanic arc origin. Sepiolite zircon also has dominantly negative  $\epsilon\text{Hf}_0$  values, but maximum values of  $\epsilon\text{Hf}_0$  reach  $+11$  (Andrews et al. 2016). Attapulgite-derived zircon is thus more easily distinguished as a contaminant of zircon from young, mantle-derived igneous rocks typical for IODP drilling than sepiolite-derived zircon.

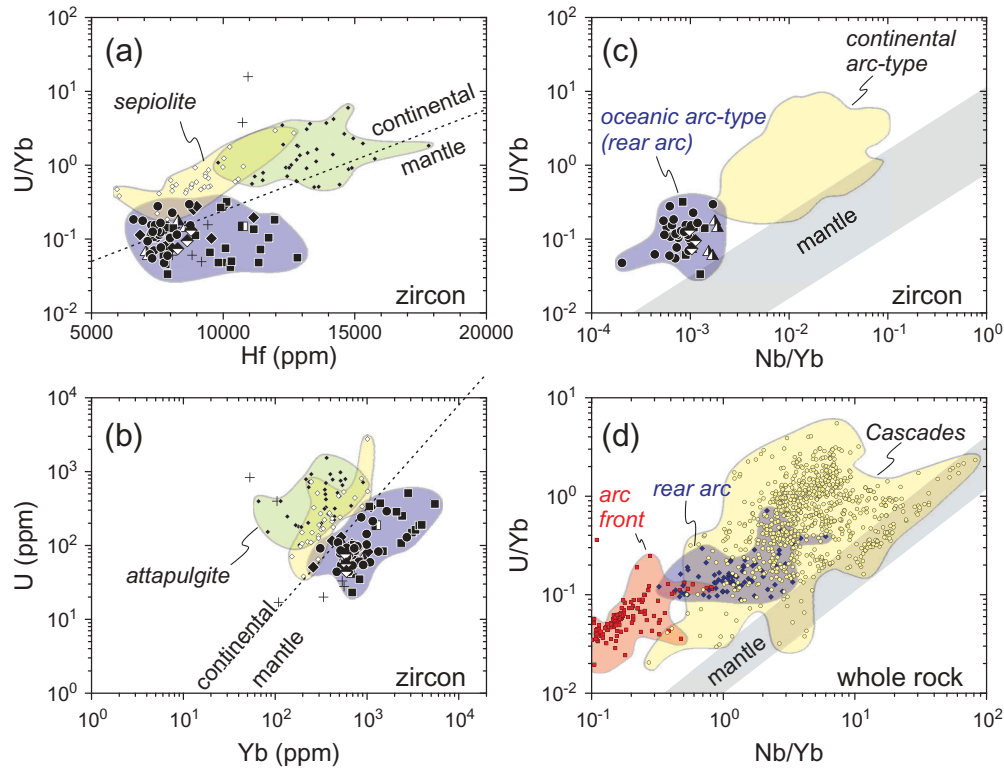


**Figure 8.** (a–c) Trace element characteristics of Lzu zircon in comparison with compositional fields for zircon oceanic environments (mid-ocean ridges, oceanic islands) and fields for continental arcs (Grimes *et al.* 2015). (d) Literature data plotted for comparison compiling whole-rock data for Lzu arc front and rear arc (see caption Figure 3) and the Cascades arc (precompiled in GEOROC; [http://georoc.mpch-mainz.gwdg.de/georoc/Csv\\_Downloads/Convergent\\_Margins\\_comp/CASCADES.csv](http://georoc.mpch-mainz.gwdg.de/georoc/Csv_Downloads/Convergent_Margins_comp/CASCADES.csv); accessed January 21 2017). Unit symbols as in Figure 6; sepiolite and attapulgitite drill mud data plotted with small open and filled symbols, respectively.

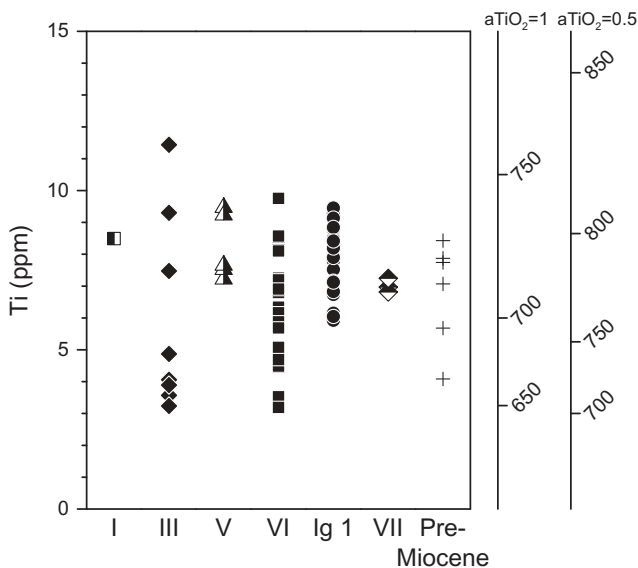


**Figure 9.** Summary of Ti-in-zircon results with temperatures calculated for titanium activities  $a_{\text{TiO}_2}$  between 0.5 and 1 using the calibration of Ferry and Watson (2007). Activity of silica ( $a_{\text{SiO}_2}$ ) = 1. Unit symbols as in Figure 6. Pre-Miocene zircon includes potential contaminants from attapulgitite and sepiolite drill mud and zircon of unknown provenance.

## Discussion

### Expanded age model for Site U1437

New radiometric ages reveal the absence of any major age hiatus for Site U1437 to a depth of ~1656 mbsf (Figure 2). This includes the single zircon from Sample 350-U1437E-62R-5, 60–65 cm, which we interpret as associated with rear-arc volcanism based on its trace element, oxygen, and hafnium isotopic compositions, which match those of Miocene zircon crystals recovered upsection. Unfortunately,  $^{40}\text{Ar}/^{39}\text{Ar}$  ages of Unit VII are unreliable, presumably due to later hydrothermal overprint. The concordant plateaus from most samples from below Ig 1 show that hydrothermal alteration caused replacement of K and/or Ca, coupled with degassing of Ar. This is similar to what was observed in some lavas from ODP Sites 786 and 782 on the arc front (Cosca *et al.* 1998). The recorded apparent ages likely represent the time in which the system cooled to below the plagioclase closure temperature (ca. 225°C; Cassata *et al.* 2009). The atmospheric  $^{40}\text{Ar}/^{36}\text{Ar}$  intercepts also show that hydrothermal fluids were likely meteoric as opposed

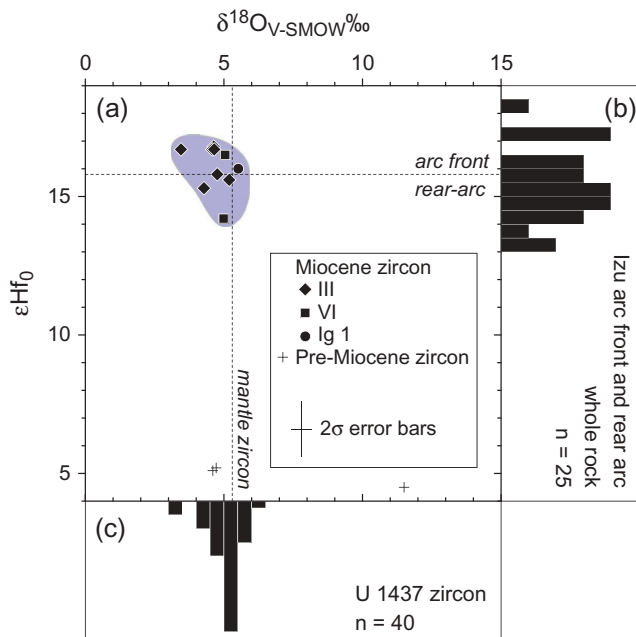


**Figure 10.** (a) Oxygen ( $\delta^{18}\text{O}$  relative to Vienna Standard Mean Ocean Water V-SMOW) versus hafnium isotopic compositions ( $\epsilon\text{Hf}_0$  = present day) of Site U1437 zircon. Dashed lines indicate mantle  $\delta^{18}\text{O}$  value of  $5.3 \pm 0.3\text{‰}$  (Valley 2003) and the boundary between  $\epsilon\text{Hf}$  values for Izu arc-front and rear-arc lavas (Tamura *et al.* 2007; Tollstrup *et al.* 2010). (b) Histogram showing whole-rock Hf isotopic compositions from the literature (references see above). (c) Histogram of all  $\delta^{18}\text{O}$  analyses of Site U1437 zircon.

to magmatic. These hydrothermally altered  $^{40}\text{Ar}/^{39}\text{Ar}$  ages, in combination with the extreme scarcity of zircon, still leaves uncertainty regarding the age of Unit VII below  $\sim 1656$  mbsf. Extrapolating the  $^{40}\text{Ar}/^{39}\text{Ar}$  age of Unit I and the sole zircon age for Unit VII (Sample 350-U1437E-62R-5, 60–65 cm) yields a tentative age estimate of ca. 17 Ma for the bottom of Hole U1437E at 1806.5 mbsf. This is intriguing because minor deepening of the Hole U1437E during a future expedition might penetrate rocks predating the ca. 17 Ma (re-)organization of the Neogene arc.

There is an enigmatic U–Pb age of ca. 51 Ma from a single zircon of Sample 350-U1437E-70R-3, 62–134 cm (1720 mbsf), which was analysed in duplicate targeting core and outer domains. This grain also has extremely low Th/U (0.06), comparatively high  $\delta^{18}\text{O}$  (11‰), and low  $\epsilon\text{Hf}$  (+6, initial value calculated for 51 Ma). These characteristics combined suggest a metamorphic origin, and we thus interpret this crystal as being unrelated to the emplacement of its host deposits. Because this age does not match the zircon age spectrum for sepiolite (Andrews *et al.* 2016) or attapulgite drill mud (see below), it is unlikely a drilling contaminant, and because of the new equipment used during zircon processing, we also dismiss laboratory contamination. Although it is

intriguing that this age coincides with subduction initiation along the Izu-Bonin arc (Ishizuka *et al.* 2011), we exclude this single crystal of unresolved origin as an anchor for the age model of Site U1437.

### Petrogenetic implications of Site U1437 zircon data

#### Zircon drill mud contamination: evidence and mitigation

The absence of zircon in heavy mineral separates from most samples from Site U1437 indicates that sample processing was unaffected by laboratory contamination, and similar yields in successfully recovered zircon crystals by the two consortia argue against laboratory bias, both with regard to the capability to extract zircon, and the absence of laboratory contamination. There are, however, two samples where drill mud contamination is suspected based on the occurrence of zircon crystals with U–Pb ages of ca. 560 Ma and 1.1 Ga, which match peaks in the attapulgite and sepiolite zircon age spectra. Both ages are also prevalent in detrital zircon age populations from North America and are related to Neo- and Mesoproterozoic collisional orogenies (Gehrels and Pecha 2014). Because of their comparatively large grain size ( $\sim 100 \mu\text{m}$ ), these crystals are unlikely to be transported in suspension by oceanic currents, and we therefore suspect an origin as drill mud contamination from attapulgite quarried in southeastern North America. There are a few additional zircon crystals with unusual ages: two crystals are from evolved tuff Sample 350-U1437D-63R-1, 63–90 cm, which yielded concordant U–Pb ages of ca. 250 Ma, and a single ca. 51 Ma zircon from Sample 350-U1437E-70R-3, 62–134 cm (already discussed in the previous section). These zircon crystals are also large ( $\sim 100 \mu\text{m}$ ), and they have a ‘continental’ trace element and isotopic affinity, but their ages are atypical for the attapulgite and sepiolite zircon spectra. Their origins presently remain enigmatic. We are, however, confident that the remainder of zircon crystals recovered from Site U1437 originated *in situ* in the Izu rear arc, and we rule out drilling or laboratory contamination based on the combined evidence of geochronology, trace element, oxygen, and hafnium isotopic data.

#### Evolved melt generation and zircon crystallization in the Izu rear arc

The recovery of zircon from lapilli-tuffs (mainly of Unit VI) and Igneous Unit Ig 1 suggests that they originated from proximal vents in the Izu rear arc, notwithstanding the lack of zircon in lapilli-tuffs tentatively correlated to seamounts Meireki and Daigo-Nishi-Aogashima Knoll (Unit II) and Manji (Unit IV). Geochemical data provide

some indication as to why this absence of zircon in comparatively evolved seamount lavas is not entirely surprising. Shipboard whole-rock geochemical data for Units II and IV lapilli-tuffs indicate comparatively low SiO<sub>2</sub> abundances (62–68 wt.% and 49–61 wt.%, respectively; Tamura *et al.* 2015); Zr abundances (133–202 ppm and 60–190 ppm) are elevated compared to most evolved lavas from the arc front (Figure 4), but mostly lower than upper continental crustal values (193 ppm; Rudnick and Gao 2003). The whole-rock analyses of volcanoclastic intervals from Site U1437 cannot be used as a reliable proxy for major element magma compositions due to impurities (e.g. polymictic clasts, marine carbonates) and alteration. We thus modelled magmatic trends for Site U1437 samples using the abundant published data for arc front lavas, and generated trends in *M* versus SiO<sub>2</sub> to estimate *M* for a given SiO<sub>2</sub> (after normalization to 100% without loss on ignition LOI; Figure 4). Note that *M*-values for rear-arc lavas show a similar evolution as the arc front lavas, but less data are available, and we thus prefer *M* versus SiO<sub>2</sub> as calculated for arc front lavas. For rear-arc lavas with SiO<sub>2</sub> > 62 wt.%, SiO<sub>2</sub> and Zr abundances are inversely correlated, suggesting zircon fractionation at saturation temperatures of 700°C, but melts at lower SiO<sub>2</sub> or higher temperature were likely zircon undersaturated. The two samples that yielded most zircon crystals (Sample 350-U1437E-32R-3, 7–29 cm, lapilli-tuff from Unit VI, and Sample 350-U1437E-35R-1, 83–85 cm, Igneous Unit Ig 1) broadly follow this trend. The absence of a kinked trend in Zr versus SiO<sub>2</sub> for the arc front lavas could indicate that these melts reached zircon saturation late or not at all, reflecting the lower initial Zr abundances in basaltic parental magmas in the arc front compared to the rear arc.

Although zircon is rare in Site U1437 rocks, zircon-bearing hornblende-biotite granodiorites have been reported for the Izu rear arc where they were robotically retrieved from water depths between 462 and 1277 mbsf along the flanks of Daisan West Sumisu Knoll (Tani *et al.* 2015). This knoll forms the eastern terminus of the Enpo rear-arc seamount chain where it intersects the arc-parallel extensional zone. U–Pb zircon ages are mostly ca. 2.6 Ma with some crystal interiors yielding ages between ca. 8.6 and 8.2 Ma (Tani *et al.* 2015). U abundances in these zircon crystals (average 190 ppm) are slightly higher than those for Site U1437. Elevated U in plutonic zircon might reflect crystallization from evolved interstitial melts during crystallization at depth, whereas volcanic zircon might represent earlier stages of differentiation. The host granodiorites on average have SiO<sub>2</sub> abundances of ~70 wt.% and Zr = 132 ppm. This is consistent with the trend for

rear-arc magmas, suggesting that zircon saturation was reached comparatively late in the evolution of rear-arc magmas, and that zircon ultimately crystallized upon cooling and differentiation in subvolcanic magma reservoirs. Thus, although comparatively scarce in volcanic samples, zircon is likely a common accessory mineral in mid-crustal intrusions of the Izu rear arc. Similarly, the Cretaceous Alisitos arc field analog to the extensional zone in the Izu arc has scarce volcanic zircon and abundant plutonic zircon (Medynski *et al.* 2016). The preservation of cores likely inherited from pre-existing crust in Daisan West Sumisu Knoll zircon crystals supports this notion (Tani *et al.* 2015).

### **Trace element composition of Site U1437 intra-oceanic arc zircon in a global comparison**

Zircon sources can be discriminated based on trace element compositions, which is useful if zircon occurs not in its original magmatic context, or if the host rocks have become altered. Source classifications (Grimes *et al.* 2007, 2015; Carley *et al.* 2014) have been devised based on analysis of zircon from known tectono-magmatic environments. Some trace elements are directly temperature-dependent and therefore reliable indicators of fractional crystallization, as indicated by the covariation of Ti-in-zircon and Zr/Hf. Other controlling parameters are fractional crystallization of major and accessory minerals: amphibole, for example, has comparatively high partitioning values for MREE and HREE so that U/Yb will increase when amphibole is present during fractional crystallization. Early-crystallizing zircon will deplete the remaining melt (and subsequently crystallized zircon) in HREE, as will apatite and titanite, but not so for the MREE. Titanite and ilmenite also have high partitioning coefficient (*D*) values for Nb. Collectively, these effects can mask different source characteristics, such as low U/Yb in depleted mantle versus high U/Yb in continental crust. The presence or absence of different mineral phases during fractional crystallization can also exacerbate differences in trace element behaviour. For example, when amphibole is present during differentiation in continental arcs, melts evolve to higher U/Yb. This contrasts with melts generated via amphibole-absent fractional crystallization, such as MOR or OIB settings (Grimes *et al.* 2015).

Nb/Yb in zircon is a useful discriminant for zircon sources, as both elements are insensitive to oxidation state, and the ratio is invariant during differentiation from basalt to dacite (e.g. Wanless *et al.* 2010). Based on the compilation of zircon Nb/Yb from different magmatic tectonic environments, and whole-rock data from the literature (Wanless *et al.* 2010 for MOR; Padilla *et al.*



2016 for Iceland; Cousens *et al.* 2003 for Hawaii; Rudnick and Gao 2003 for continental crustal average), the zircon-melt partitioning coefficient ratio  $D_{\text{Nb}}/D_{\text{Yb}}$  is between 0.001 and 0.008. Using these  $D$  values, the Site U1437 zircon data translate to melt Nb/Yb of ~0.1–0.9. This is between the averages for modern Izu arc front lavas (~0.2) and Izu rear-arc rocks (~1.5). Trace elements for zircon from Izu arc front lavas are lacking, but from extrapolation of whole-rock trends we predict that these would have even lower Nb/Yb (and U/Yb) than zircon from the Izu rear arc (Figure 8).

Existing chemical classifications for zircon origins largely exclude oceanic arcs (cf. Barth *et al.* 2017). Based on global trends for arc *versus* mantle magmas, Grimes *et al.* (2015) postulated that such zircon will extend the trend for continental arcs to lower U/Yb and lower Nb/Yb, analogous to oceanic arc lavas having lower U/Yb and Nb/Yb than continental arc lavas (e.g. Pearce 2008). Compared to Izu arc front lavas, the Izu rear-arc lavas, however, are less depleted in Nb and U relative to Yb (Figure 8). Consistent with whole-rock trends, zircon compositions for Site U1437 plot at lower U/Yb relative to continental arcs, but have higher U/Yb at a given Nb/Y than most MOR zircon (Figure 8). Although no other oceanic arc zircon is included in the compilation of Grimes *et al.* (2015), there are similarities between Site U1437 zircon trace elemental patterns and those of zircon from supra-subduction ophiolites. This implies that zircon trace element compositions can distinguish oceanic from continental arc sources, as well as discriminate zircon from mantle sources in the absence of subduction.

### **Intra-oceanic arcs and continental crust formation: IBM zircon in comparison with Hadean detrital zircon**

Intra-oceanic arc crust is widely considered as a building block for the construction of continental crust, based on the broad compositional similarities between magmatism in extant intra-oceanic arcs and continental crustal averages (e.g. Rudnick and Gao 2003; Stern and Scholl 2010). Chemical evidence is supported by seismology where mid-crustal layers in modern arcs have seismic velocities resembling igneous (I)-type intrusive plutonic suites in fossil arc terranes accreted to cratonic crust in regions with a protracted subduction history (e.g. Suyehiro *et al.* 1996; Hacker *et al.* 2008). Models for ‘continentalization’ of arc crust postulate intra-crustal modification, including partial remelting of originally basaltic crust derived from the subarc mantle wedge to form granitic rocks, as well as foundering of ultramafic restite into the mantle (e.g. Tatsumi 2005; Stern

and Scholl 2010). There are, however, discrepancies between prevailing low-K intra-oceanic arc magmatic suites (ranging from basalt to rhyolite; e.g. Tamura *et al.* 2009) on one hand, and the dominantly granodioritic compositions of I-type plutons (e.g. Tani *et al.* 2015) and continental crustal average on the other. Plutonic rocks exposed in fossil arcs (Gill and Stork 1979; Haraguchi *et al.* 2003; Greene *et al.* 2006) are also tonalitic (i.e. low-K), and thus distinct from granodioritic continental averages. Global correlations between K contents of arc magmas and  $h$  (the depth to the Wadati-Benioff seismogenic zone; Dickinson and Hatherton 1967; Dickinson 1975) imply that magmatic addition in the rear arc may be an important, but thus far overlooked component in the construction of intra-oceanic arcs with continental crustal affinities.

Hadean zircon has been recovered as xenocrysts from orthogneissic rocks in various locations (e.g. Western Australia; Nelson *et al.* 2000; West Greenland; Mojzsis and Harrison 2002, and Northern Canada; Iizuka *et al.* 2006), but they are mostly known as detrital crystals in metaconglomerates from Western Australia (Harrison 2009), which were deposited before ca. 2.65–3.0 Ga (Rasmussen *et al.* 2010). Because zircon crystals occur separated from their magmatic sources, trace elemental and isotopic compositions are essential to establish the chemical nature of their igneous protoliths and their affinities to continental crust (e.g. Bell *et al.* 2016). Zircon trace element data from modern magmatic environments have been used to delineate possible magmatic sources for the Hadean zircon record. Carley *et al.* (2014) dismissed differentiated melts from an enriched mantle source equivalent to Iceland as a potential analogue for the Hadean zircon. The comparison between Izu rear-arc zircon and lava compositions suggests that zircon faithfully records characteristic trace element ratios of their magmatic sources. Izu rear-arc zircon, however, is considerably lower in U/Yb and Nb/Yb compared to the Hadean population, which more closely overlaps with the field for continental arc zircon (Figure 11). Metamictization of Hadean zircon would preferentially eliminate high-U zircon, and thus likely bias against high U/Yb crystals, further enhancing the differences between the Hadean zircon population and the Izu rear-arc zircon. Regardless of these differences, both populations, Izu rear-arc and Hadean zircon, fall above the main mantle zircon trend. This indicates that fluid/melt mobile elements (e.g. Kessel *et al.* 2005) were enriched above mantle values in the sources of Izu rear-arc and Hadean magmas. The Hadean zircon trace element record is thus consistent with a contribution of hydrous fluids or melts similar to those formed during subduction in modern

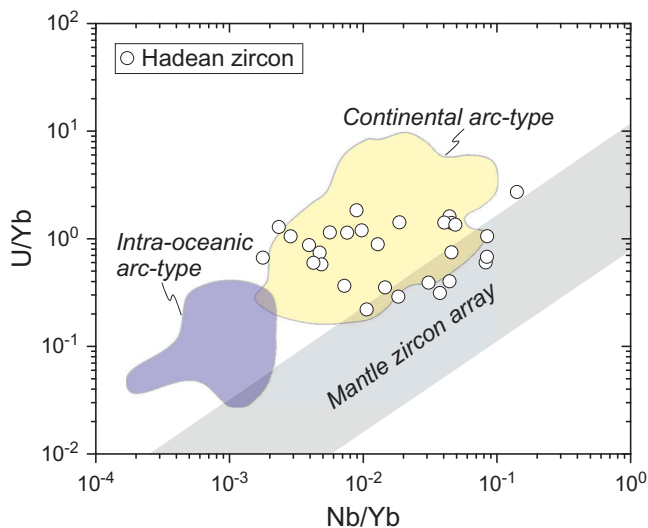


**Figure 11.** Comparison of zircon trace element data for continental (compiled by Grimes *et al.* 2015) and intra-oceanic (this study) arc settings. Data for Hadean zircon from Crowley *et al.* (2005) and Peck *et al.* (2001) from the compilation of Carley *et al.* (2014) are plotted for comparison.

environments, but has more affinity to continental than intra-oceanic arcs.

## Conclusions

Radiometric dating ( $^{40}\text{Ar}/^{39}\text{Ar}$ , U–Pb) of volcanoclastic deposits and one rhyolite sill recovered by deep-sea drilling in the Izu rear arc (IODP Site U1437) indicates ages between ca. 4 and 15 Ma. These ages overlap with bio- and magnetostratigraphic constraints for the shallower (<1302 mbsf) part of the core, but because of the scarcity of zircon and pervasive alteration no reliable radiometric ages were obtained for depths >1656 mbsf. This presently leaves the last 150 m of Site U1437 undated. We also present evidence for occasional contamination of samples through zircon derived from attapulgite and sepiolite drill muds, but we can confidently identify these contaminants based on their older ages, coupled with continent-like trace elements, and O- and Hf-isotopic compositions. Zircon crystals in pyroclastic rocks from Site U1437 are likely locally derived, based on their association with lapilli- and block-sized juvenile clasts. Zircon Hf isotopic compositions for Site U1437 samples are slightly lower than those expected for zircon from the modern arc front, and their trace elements mirror the more enriched signatures of the rear arc relative to the arc front. Zircon oxygen isotopic compositions are broadly mantle-like. These relations indicate that zircon can be a faithful indicator of magmatic provenance from different segments of intra-oceanic arcs, and that differences in magmatic

compositions between arc front and rear arc persisted through time. This further encourages using zircon trace elements in Hadean detrital zircon to trace their tectono-magmatic provenance.

## Acknowledgments

The ion microprobe facility at UCLA is partly supported by a grant from the NSF Instrumentation and Facilities Program, Division of Earth Sciences, National Science Foundation. A new mineral separation facility at CSUB was made possible by NSF. Zircon work was supported by IODP Post-Expedition Awards to Schmitt (UCLA), Andrews (CSUB) and Busby (UC Davis). Argon geochronology work was supported by IODP Post-Expedition Award to Koppers (OSU).

## Disclosure statement

No potential conflict of interest was reported by the authors.

## Funding

This work was supported by NSF Post-expedition activity (PEA) awards to Andrews, Busby, Koppers, and Schmitt, and NSF award HRD 1137774.

## References

- Amelin, Y., and Davis, W.J., 2005, Geochemical test for branching decay of  $^{176}\text{Lu}$ : *Geochimica et Cosmochimica Acta*, v. 69, p. 465–473. doi:10.1016/j.gca.2004.04.028
- Anders, E., and Grevesse, N., 1989, Abundances of the elements: Meteoritic and solar: *Geochimica et Cosmochimica Acta*, v. 53, no. 1, p. 197–214. doi:10.1016/0016-7037(89)90286-X
- Andrews, G.D.M., Schmitt, A.K., Busby, C.J., Brown, S.R., Blum, P., and Harvey, J., 2016, Age and compositional data of zircon from sepiolite drilling mud to identify contamination of ocean drilling samples: *Geochemistry, Geophysics, Geosystems*, v. 17, no. 8, p. 3512–3526. doi:10.1002/2016GC006397
- Arculus, R.J., Ishizuka, O., Bogus, K.A., Gurnis, M., Hickey-Vargas, R., Aljehdali, M.H., Bandini-Maeder, A.N., Barth, A. P., Brandl, P.A., Drab, L., Do Monte Guerra, R., Hamada, M., Jiang, F., Kanayama, K., Kender, S., Kusano, Y., Li, H., Loudin, L.C., Maffione, M., Marsaglia, K.M., McCarthy, A., Meffre, S., Morris, A., Neuhaus, M., Savov, I.P., Sena, C., Tepley, III, F.J., van der Land, C., Yogodzinski, G.M., and Zhang, Z., 2015, A record of spontaneous subduction initiation in the Izu-Bonin-Mariana arc: *Nature Geoscience*, v. 8, no. 9, p. 728–733. doi:10.1038/ngeo2515
- Bacon, C.R., 1989, Crystallization of accessory phases in magmas by local saturation adjacent to phenocrysts: *Geochimica et Cosmochimica Acta*, v. 53, no. 5, p. 1055–1066. doi:10.1016/0016-7037(89)90210-X
- Baertschi, P., 1976, Absolute  $^{18}\text{O}$  content of standard mean ocean water: *Earth and Planetary Science Letters*, v. 31, no. 3, p. 341–344. doi:10.1016/0012-821X(76)90115-1
- Balbas, A., Koppers, A.A., Kent, D.V., Konrad, K., and Clark, P.U., 2016, Identification of the short-lived Santa Rosa

- geomagnetic excursion in lavas on Floreana Island (Galapagos) by  $^{40}\text{Ar}/^{39}\text{Ar}$  geochronology: *Geology*, v. 44, no. 5, p. 359–362. doi:[10.1130/G37569.1](https://doi.org/10.1130/G37569.1)
- Barth, A.P., Tani, K., Meffre, S., Wooden, J.L., Coble, M.A., Arculus, R.J., Ishizuka, O., and Shukle, J., 2017, Generation of silicic melts in the early Izu-Bonin arc recorded by detrital zircons in proximal arc volcanoclastic rocks from the Philippine Sea: *Geochemistry, Geophysics, Geosystems*. doi: [10.1002/2017GC006948](https://doi.org/10.1002/2017GC006948)
- Bell, E.A., Boehnke, P., and Harrison, T.M., 2016, Recovering the primary geochemistry of Jack Hills zircons through quantitative estimates of chemical alteration: *Geochimica et Cosmochimica Acta*, v. 191, p. 187–202. doi:[10.1016/j.gca.2016.07.016](https://doi.org/10.1016/j.gca.2016.07.016)
- Black, L.P., Kamo, S.L., Allen, C.M., Davis, D.W., Aleinikoff, J.N., Valley, J.W., Mundil, R., Campbell, I.H., Korsch, R.J., Williams, I.S., and Foudoulis, C., 2004, Improved  $^{206}\text{Pb}/^{238}\text{U}$  microprobe geochronology by the monitoring of a trace-element related matrix effect; SHRIMP, ID-TIMS, ELA-ICP-MS, and oxygen isotope documentation for a series of zircon standards: *Chemical Geology*, v. 205, p. 115–140. doi:[10.1016/j.chemgeo.2004.01.003](https://doi.org/10.1016/j.chemgeo.2004.01.003)
- Blundy, J., and Wood, B., 2003, Mineral-melt partitioning of uranium, thorium and their daughters: *Reviews in Mineralogy and Geochemistry*, v. 52, no. 1, p. 59–123. doi:[10.2113/0520059](https://doi.org/10.2113/0520059)
- Boehnke, P., Watson, E.B., Trail, D., Harrison, T.M., and Schmitt, A.K., 2013, Zircon saturation re-visited: *Chemical Geology*, v. 351, p. 324–334. doi:[10.1016/j.chemgeo.2013.05.028](https://doi.org/10.1016/j.chemgeo.2013.05.028)
- Bouvier, A., Vervoort, J.D., and Patchett, P.J., 2008, The Lu–Hf and Sm–Nd isotopic composition of CHUR: Constraints from unequilibrated chondrites and implications for the bulk composition of terrestrial planets: *Earth and Planetary Science Letters*, v. 273, no. 1–2, p. 48–57. doi:[10.1016/j.epsl.2008.06.010](https://doi.org/10.1016/j.epsl.2008.06.010)
- Busby, C.J., Tamura, Y., Blum, P., Guèrin, G., Andrews, G.D.M., Barker, A.K., Berger, J.L.R., Bongioiolo, E.M., Bordiga, M., DeBari, S.M., Gill, J.B., Hamelin, C., Jia, J., John, E.H., Jonas, A.-S., Jutzeler, M., Kars, M.A.C., Kita, Z.A., Konrad, K., Mahony, S.H., Martini, M., Miyazaki, T., Musgrave, R.J., Nascimento, D.B., Nichols, A.R.L., Ribeiro, J.M., Sato, T., Schindlbeck, J.C., Schmitt, A.K., Straub, S.M., Vautravers, M. J., and Yang, Y., 2017, The missing half of the subduction factory: Shipboard results from the Izu rear arc, IODP expedition 350: *International Geology Review*, p. 1–32. doi:[10.1080/00206814.2017.1292469](https://doi.org/10.1080/00206814.2017.1292469)
- Busby-Spera, C.J., and White, J.D., 1987, Variation in peperite textures associated with differing host-sediment properties: *Bulletin of Volcanology*, v. 49, no. 6, p. 765–776. doi:[10.1007/BF01079827](https://doi.org/10.1007/BF01079827)
- Carley, T.L., Miller, C.F., Wooden, J.L., Padilla, A.J., Schmitt, A.K., Economos, R.C., Bindeman, I.N., and Jordan, B.T., 2014, Iceland is not a magmatic analog for the Hadean: Evidence from the zircon record: *Earth and Planetary Science Letters*, v. 405, p. 85–97. doi:[10.1016/j.epsl.2014.08.015](https://doi.org/10.1016/j.epsl.2014.08.015)
- Cassata, W.S., Renne, P.R., and Shuster, D.L., 2009, Argon diffusion in plagioclase and implications for thermochronometry: A case study from the Bushveld Complex, South Africa: *Geochimica et Cosmochimica Acta*, v. 73, no. 21, p. 6600–6612. doi:[10.1016/j.gca.2009.07.017](https://doi.org/10.1016/j.gca.2009.07.017)
- Cosca, M., Arculus, R., Pearce, J., and Mitchell, J., 1998,  $^{40}\text{Ar}/^{39}\text{Ar}$  and K–Ar geochronological age constraints for the inception and early evolution of the Izu–Bonin–Mariana arc system: *The Island Arc*, v. 7, no. 3, p. 579–595. doi:[10.1111/iar.1998.7.issue-3](https://doi.org/10.1111/iar.1998.7.issue-3)
- Cousens, B.L., Clague, D.A., and Sharp, W.D., 2003, Chronology, chemistry, and origin of trachytes from Hualalai Volcano, Hawaii: *Geochemistry, Geophysics, Geosystems*, 4, no. 9. doi:[10.1029/2003GC000560](https://doi.org/10.1029/2003GC000560)
- Crowley, J.L., Myers, J.S., Sylvester, P.J., and Cox, R.A., 2005, Detrital zircon from the Jack Hills and Mount Narryer, Western Australia: Evidence for diverse >4.0 Ga source rocks: *The Journal of Geology*, v. 113, no. 3, p. 239–263. doi:[10.1086/428804](https://doi.org/10.1086/428804)
- Dickinson, W.R., 1975, Potash-depth (Kh) relations in continental margin and intra-oceanic magmatic arcs: *Geology*, v. 3, no. 2, p. 53–56. doi:[10.1130/0091-7613\(1975\)3<53:PKRICM>2.0.CO;2](https://doi.org/10.1130/0091-7613(1975)3<53:PKRICM>2.0.CO;2)
- Dickinson, W.R., and Hatherton, T., 1967, Andesitic volcanism and seismicity around the Pacific: *Science*, v. 157, no. 3790, p. 801–803. doi:[10.1126/science.157.3790.801](https://doi.org/10.1126/science.157.3790.801)
- Doherty, W., 1989, An internal standardization procedure for the determination of yttrium and the rare earth elements in geological materials by inductively coupled plasma-mass spectrometry: *Spectrochimica Acta Part B: Atomic Spectroscopy*, v. 44, p. 263–280. doi:[10.1016/0584-8547\(89\)80031-X](https://doi.org/10.1016/0584-8547(89)80031-X)
- Ferry, J., and Watson, E., 2007, New thermodynamic models and revised calibrations for the Ti-in-zircon and Zr-in-rutile thermometers: *Contributions to Mineralogy and Petrology*, v. 154, no. 4, p. 429–437. doi:[10.1007/s00410-007-0201-0](https://doi.org/10.1007/s00410-007-0201-0)
- Fu, B., Page, F.Z., Cavosie, A.J., Fournelle, J., Kita, N.T., Lackey, J. S., Wilde, S.A., and Valley, J.W., 2008, Ti-in-zircon thermometry: Applications and limitations: *Contributions to Mineralogy and Petrology*, v. 156, no. 2, p. 197–215. doi:[10.1007/s00410-008-0281-5](https://doi.org/10.1007/s00410-008-0281-5)
- Gehrels, G., and Pecha, M., 2014, Detrital zircon U–Pb geochronology and Hf isotope geochemistry of Paleozoic and Triassic passive margin strata of western North America: *Geosphere*, v. 10, no. 1, p. 49–65. doi:[10.1130/GES00889.1](https://doi.org/10.1130/GES00889.1)
- Gill, J., and Stork, A., 1979, Miocene low-K dacites and trondhjemitic rocks of Fiji: *Trondhjemitic, dacites and related rocks*: Amsterdam, Elsevier, p. 629–649.
- Greene, A.R., DeBARI, S.M., Kelemen, P.B., Blusztajn, J., and Clift, P.D., 2006, A detailed geochemical study of island arc crust: The Talkeetna Arc section, south-central Alaska: *Journal of Petrology*, v. 47, no. 6, p. 1051–1093. doi:[10.1093/ptrology/egl002](https://doi.org/10.1093/ptrology/egl002)
- Grimes, C., Wooden, J., Cheadle, M., and John, B., 2015, “Fingerprinting” tectono-magmatic provenance using trace elements in igneous zircon: *Contributions to Mineralogy and Petrology*, v. 170, no. 5–6, p. 46. doi:[10.1007/s00410-015-1199-3](https://doi.org/10.1007/s00410-015-1199-3)
- Grimes, C.B., John, B.E., Kelemen, P., Mazdab, F., Wooden, J., Cheadle, M.J., Hanghøj, K., and Schwartz, J., 2007, Trace element chemistry of zircons from oceanic crust: A method for distinguishing detrital zircon provenance: *Geology*, v. 35, no. 7, p. 643–646. doi:[10.1130/G23603A.1](https://doi.org/10.1130/G23603A.1)
- Hacker, B.R., Mehl, L., Kelemen, P.B., Rioux, M., Behn, M.D., and Luffi, P., 2008, Reconstruction of the Talkeetna intraoceanic arc of Alaska through thermobarometry: *Journal of Geophysical Research: Solid Earth*, 113, no. B3. doi:[10.1029/2007JB005208](https://doi.org/10.1029/2007JB005208)
- Haraguchi, S., Ishii, T., Kimura, J.-I., and Ohara, Y., 2003, Formation of tonalite from basaltic magma at the

- Komahashi-Daini Seamount, northern Kyushu-Palau Ridge in the Philippine Sea, and growth of Izu-Ogasawara (Bonin)-Mariana arc crust: Contributions to Mineralogy and Petrology, v. 145, no. 2, p. 151–168. doi:10.1007/s00410-002-0433-y
- Harrison, T.M., 2009, The Hadean crust: Evidence from >4 Ga zircons: Annual Review of Earth and Planetary Sciences, v. 37, p. 479–505. doi:10.1146/annurev.earth.031208.100151
- Hiess, J., Nutman, A.P., Bennett, V.C., and Holden, P., 2008, Ti-in-zircon thermometry applied to contrasting Archean metamorphic and igneous systems: Chemical Geology, v. 247, no. 3, p. 323–338. doi:10.1016/j.chemgeo.2007.10.012
- Hochstaedter, A., Gill, J., Peters, R., Broughton, P., Holden, P., and Taylor, B., 2001, Across-arc geochemical trends in the Izu-Bonin arc: Contributions from the subducting slab: Geochemistry, Geophysics, Geosystems, 2, no. 7. doi:10.1029/2000GC000105
- Hochstaedter, A.G., Gill, J.B., and Morris, J.D., 1990, Volcanism in the Sumisu Rift, II. Subduction and non-subduction related components: Earth and Planetary Science Letters, v. 100, no. 1–3, p. 195–209. doi:10.1016/0012-821X(90)90185-Z
- Hochstaedter, A.G., Gill, J.B., Taylor, B., Ishizuka, O., Yuasa, M., and Monta, S., 2000, Across-arc geochemical trends in the Izu-Bonin arc: Constraints on source composition and mantle melting: Journal of Geophysical Research: Solid Earth, v. 105, no. B1, p. 495–512. doi:10.1029/1999JB900125
- Horie, K., Takehara, M., Suda, Y., and Hidaka, H., 2013, Potential Mesozoic reference zircon from the Unazuki plutonic complex: Geochronological and geochemical characterization: The Island Arc, v. 22, p. 292–305. doi:10.1111/iar.2013.22.issue-3
- Hoskin, P.W., and Schaltegger, U., 2003, The composition of zircon and igneous and metamorphic petrogenesis: Reviews in Mineralogy and Geochemistry, v. 53, no. 1, p. 27–62. doi:10.2113/0530027
- Ickert, R., Hiess, J., Williams, I., Holden, P., Ireland, T., Lanc, P., Schram, N., Foster, J., and Clement, S., 2008, Determining high precision, in situ, oxygen isotope ratios with a SHRIMP II: Analyses of MPI-DING silicate-glass reference materials and zircon from contrasting granites: Chemical Geology, v. 257, no. 1–2, p. 114–128. doi:10.1016/j.chemgeo.2008.08.024
- Ishizuka, T., Horie, K., Komiya, T., Maruyama, S., Hirata, T., Hidaka, H., and Windley, B.F., 2006, 4.2 Ga zircon xenocryst in an Acasta gneiss from northwestern Canada: Evidence for early continental crust: Geology, v. 34, no. 4, p. 245–248. doi:10.1130/G22124.1
- Ishizuka, O., Kimura, J.-I., Li, Y.B., Stern, R.J., Reagan, M.K., Taylor, R.N., Ohara, Y., Bloomer, S.H., Ishii, T., and Hargrove, U.S., 2006a, Early stages in the evolution of Izu-Bonin arc volcanism: New age, chemical, and isotopic constraints: Earth and Planetary Science Letters, v. 250, no. 1, p. 385–401. doi:10.1016/j.epsl.2006.08.007
- Ishizuka, O., Tani, K., Reagan, M.K., Kanayama, K., Umino, S., Harigane, Y., Sakamoto, I., Miyajima, Y., Yuasa, M., and Dunkley, D.J., 2011, The timescales of subduction initiation and subsequent evolution of an oceanic island arc: Earth and Planetary Science Letters, v. 306, no. 3–4, p. 229–240. doi:10.1016/j.epsl.2011.04.006
- Ishizuka, O., Taylor, R.N., Milton, J.A., and Nesbitt, R.W., 2003a, Fluid–mantle interaction in an intra-oceanic arc: Constraints from high-precision Pb isotopes: Earth and Planetary Science Letters, v. 211, no. 3–4, p. 221–236. doi:10.1016/S0012-821X(03)00201-2
- Ishizuka, O., Taylor, R.N., Milton, J.A., Nesbitt, R.W., Yuasa, M., and Sakamoto, I., 2006b, Variation in the mantle sources of the northern Izu arc with time and space—constraints from high-precision Pb isotopes: Journal of Volcanology and Geothermal Research, v. 156, no. 3–4, p. 266–290. doi:10.1016/j.jvolgeores.2006.03.005
- Ishizuka, O., Uto, K., and Yuasa, M., 2003b, Volcanic history of the back-arc region of the Izu-Bonin (Ogasawara) arc: Geological Society, London, Special Publications, v. 219, no. 1, p. 187–205. doi:10.1144/GSL.SP.2003.219.01.09
- Ishizuka, O., Uto, K., Yuasa, M., and Hochstaedter, A., 1998, K–Ar ages from seamount chains in the back-arc region of the Izu-Ogasawara arc: The Island Arc, v. 7, no. 3, p. 408–421. doi:10.1111/iar.1998.7.issue-3
- Ishizuka, O., Uto, K., Yuasa, M., and Hochstaedter, A.G., 2003c, Volcanism in the earliest stage of back-arc rifting in the Izu-Bonin arc revealed by laser-heating <sup>40</sup>Ar/<sup>39</sup>Ar dating: Journal of Volcanology and Geothermal Research, v. 120, no. 1–2, p. 71–85. doi:10.1016/S0377-0273(02)00365-7
- Ishizuka, O., Yuasa, M., and Uto, K., 2002, Evidence of porphyry copper-type hydrothermal activity from a submerged remnant back-arc volcano of the Izu-Bonin arc: Implications for the volcanotectonic history of back-arc seamounts: Earth and Planetary Science Letters, v. 198, no. 3–4, p. 381–399. doi:10.1016/S0012-821X(02)00515-0
- Johnson, D.M., Hooper, P.R., and Conrey, R.M., 1999, XRF analysis of rocks and minerals for major and trace elements on a single low dilution Li-tetraborate fused bead: Advances in X-Ray Analysis, v. 41, p. 843–867.
- Kenny, G.G., Whitehouse, M.J., and Kamber, B.S., 2016, Differentiated impact melt sheets may be a potential source of Hadean detrital zircon: Geology, v. 44, no. 6, p. 435–438. doi:10.1130/G37898.1
- Kessel, R., Schmidt, M.W., Ulmer, P., and Pettke, T., 2005, Trace element signature of subduction-zone fluids, melts and supercritical liquids at 120–180 km depth: Nature, v. 437, no. 7059, p. 724–727. doi:10.1038/nature03971
- Kimura, J.-I., Kent, A.J., Rowe, M.C., Katakuse, M., Nakano, F., Hacker, B.R., van Keken, P.E., Kawabata, H., and Stern, R.J., 2010, Origin of cross-chain geochemical variation in Quaternary lavas from the northern Izu arc: Using a quantitative mass balance approach to identify mantle sources and mantle wedge processes: Geochemistry, Geophysics, Geosystems, 11, no. 10. doi:10.1029/2010GC003050
- Kodaira, S., Sato, T., Takahashi, N., Miura, S., Tamura, Y., Tatsumi, Y., and Kaneda, Y., 2007, New seismological constraints on growth of continental crust in the Izu-Bonin intra-oceanic arc: Geology, v. 35, no. 11, p. 1031–1034. doi:10.1130/G23901A.1
- Koppers, A.A., 2002, ArArCALC—Software for <sup>40</sup>Ar/<sup>39</sup>Ar age calculations: Computers & Geosciences, v. 28, no. 5, p. 605–619. doi:10.1016/S0098-3004(01)00095-4
- Kuiper, K., Deino, A., Hilgen, F., Krijgsman, W., Renne, P., and Wijbrans, J., 2008, Synchronizing rock clocks of earth history: Science, v. 320, no. 5875, p. 500–504. doi:10.1126/science.1154339
- Kuritani, T., Yokoyama, T., Kobayashi, K., and Nakamura, E., 2003, Shift and rotation of composition trends by magma mixing: 1983 eruption at Miyake-jima Volcano, Japan:

- Journal of Petrology, v. 44, no. 10, p. 1895–1916. doi:10.1093/petrology/egg063
- Liu, Y., Hu, Z., Zong, K., Gao, C., Gao, S., Xu, J., and Chen, H., 2010, Reappraisal and refinement of zircon U-Pb isotope and trace element analyses by LA-ICP-MS: Chinese Science Bulletin, v. 55, no. 15, p. 1535–1546. doi:10.1007/s11434-010-3052-4
- Ludwig, K., 2001, Squid, a users manual: Berkeley, CA, Berkeley Geochronology Center Special Publication No. 2.
- Ludwig, K., 2008, Isoplot 3.7. A geochronological toolkit for Microsoft Excel: Berkeley, CA, Berkeley Geochronology Center Special Publication, No. 4, 77 p.
- Lukács, R., Harangi, S., Bachmann, O., Guillong, M., Danišik, M., Buret, Y., von Quadt, A., Dunkl, I., Fodor, L., Sliwinski, J., Soós, I., and Szepesi, J., 2015, Zircon geochronology and geochemistry to constrain the youngest eruption events and magma evolution of the Mid-Miocene ignimbrite flare-up in the Pannonian Basin, eastern central Europe: Contributions to Mineralogy and Petrology, v. 170, p. 1–26. doi:10.1007/s00410-015-1206-8
- Machida, S., and Ishii, T., 2003, Backarc volcanism along the en echelon seamounts: The Enpo seamount chain in the northern Izu-Ogasawara arc: Geochemistry, Geophysics, Geosystems, 4, no. 8. doi:10.1029/2003GC000554
- Machida, S., Ishii, T., Kimura, J.-I., Awaji, S., and Kato, Y., 2008, Petrology and geochemistry of cross-chains in the Izu-Bonin back arc: Three mantle components with contributions of hydrous liquids from a deeply subducted slab: Geochemistry, Geophysics, Geosystems, 9, no. 5. doi:10.1029/2007GC001641
- Mahon, K.I., 1996, The New “York” regression: Application of an improved statistical method to geochemistry: International Geology Review, v. 38, no. 4, p. 293–303. doi:10.1080/00206819709465336
- Medynski, S., Busby, C., DeBari, S.M., Morris, R., Andrews, G.D., Brown, S.R., and Schmitt, A.K., 2016, The upper-to middle-crustal section of the Alisitos Oceanic Arc, (Baja, Mexico): An analog of the Izu-Bonin-Marianas (IBM) Arc [abs.], in Fall Meeting, AGU, San Francisco, CA, 12–16 Dec 2016, p. V13C–2866.
- Min, K., Mundil, R., Renne, P.R., and Ludwig, K.R., 2000, A test for systematic errors in 40 Ar/39 Ar geochronology through comparison with U/Pb analysis of a 1.1-Ga rhyolite: Geochimica et Cosmochimica Acta, v. 64, no. 1, p. 73–98. doi:10.1016/S0016-7037(99)00204-5
- Mojzsis, S.J., and Harrison, T.M., 2002, Establishment of a 3.83-Ga magmatic age for the Akilia tonalite (southern West Greenland): Earth and Planetary Science Letters, v. 202, no. 3–4, p. 563–576. doi:10.1016/S0012-821X(02)00825-7
- Monteleone, B., Baldwin, S., Webb, L., Fitzgerald, P., Grove, M., and Schmitt, A., 2007, Late Miocene–Pliocene eclogite facies metamorphism, D’Entrecasteaux Islands, SE Papua New Guinea: Journal of Metamorphic Geology, v. 25, no. 2, p. 245–265. doi:10.1111/j.1525-1314.2006.00685.x
- Musgrave, R.J., and Kars, M., 2016, Recognizing magnetostratigraphy in overprinted and altered marine sediments: Challenges and solutions from IODP Site U1437: Geochemistry, Geophysics, Geosystems, v. 17, no. 8, p. 3190–3206. doi:10.1002/2016GC006386
- Nelson, D.R., Robinson, B.W., and Myers, J.S., 2000, Complex geological histories extending for  $\geq 4.0$  Ga deciphered from xenocryst zircon microstructures: Earth and Planetary Science Letters, v. 181, no. 1–2, p. 89–102. doi:10.1016/S0012-821X(00)00186-2
- Paces, J.B., and Miller, J.D., 1993, Precise U-Pb ages of Duluth complex and related mafic intrusions, northeastern Minnesota: Geochronological insights to physical, petrogenetic, paleomagnetic, and tectonomagmatic processes associated with the 1.1 Ga midcontinent rift system: Journal of Geophysical Research: Solid Earth, v. 98, no. B8, p. 13997–14013. doi:10.1029/93JB01159
- Padilla, A., Miller, C., Carley, T., Economos, R., Schmitt, A., Coble, M., Wooden, J., Fisher, C., Vervoort, J., and Hanchar, J., 2016, Elucidating the magmatic history of the Austurhorn silicic intrusive complex (southeast Iceland) using zircon elemental and isotopic geochemistry and geochronology: Contributions to Mineralogy and Petrology, v. 171, no. 8–9, p. 69. doi:10.1007/s00410-016-1279-z
- Patchett, P.J., 1983, Importance of the Lu-Hf isotopic system in studies of planetary chronology and chemical evolution: Geochimica et Cosmochimica Acta, v. 47, p. 81–91. doi:10.1016/0016-7037(83)90092-3
- Patchett, P.J., and Tatsumoto, M., 1981, A routine high-precision method for Lu-Hf isotope geochemistry and chronology: Contributions to Mineralogy and Petrology, v. 75, p. 263–267. doi:10.1007/BF01166766
- Pearce, J.A., 2008, Geochemical fingerprinting of oceanic basalts with applications to ophiolite classification and the search for Archean oceanic crust: Lithos, v. 100, no. 1–4, p. 14–48. doi:10.1016/j.lithos.2007.06.016
- Pearce, N.J., Perkins, W.T., Westgate, J.A., Gorton, M.P., Jackson, S.E., Neal, C.R., and Chenery, S.P., 1997, A compilation of new and published major and trace element data for NIST SRM 610 and NIST SRM 612 glass reference materials: Geostandards and Geoanalytical Research, v. 21, no. 1, p. 115–144. doi:10.1111/j.1751-908X.1997.tb00538.x
- Peck, W.H., Valley, J.W., Wilde, S.A., and Graham, C.M., 2001, Oxygen isotope ratios and rare earth elements in 3.3 to 4.4 Ga zircons: Ion microprobe evidence for high  $\delta^{18}\text{O}$  continental crust and oceans in the Early Archean: Geochimica et Cosmochimica Acta, v. 65, no. 22, p. 4215–4229. doi:10.1016/S0016-7037(01)00711-6
- Rasmussen, B., Fletcher, I.R., Muhling, J.R., and Wilde, S.A., 2010, In situ U–Th–Pb geochronology of monazite and xenotime from the Jack Hills belt: Implications for the age of deposition and metamorphism of Hadean zircons: Precambrian Research, v. 180, no. 1–2, p. 26–46. doi:10.1016/j.precamres.2010.03.004
- Reimink, J.R., Chacko, T., Stern, R.A., and Heaman, L.M., 2014, Earth’s earliest evolved crust generated in an Iceland-like setting: Nature Geoscience, v. 7, no. 7, p. 529–533. doi:10.1038/ngeo2170
- Rudnick, R., and Gao, S., 2003, Composition of the continental crust: in Holland, H.D., and Turekian, K.K., eds., Treatise on Geochemistry, Elsevier, Amsterdam, v. 3, p. 1–64.
- Schmitt, A.K., Grove, M., Harrison, T.M., Lovera, O., Hulen, J., and Walters, M., 2003, The Geysers-Cobb Mountain Magma System, California (Part 1): U-Pb zircon ages of volcanic rocks, conditions of zircon crystallization and magma residence times: Geochimica et Cosmochimica Acta, v. 67, no. 18, p. 3423–3442. doi:10.1016/S0016-7037(03)00140-6
- Shukuno, H., Tamura, Y., Tani, K., Chang, Q., Suzuki, T., and Fiske, R., 2006, Origin of silicic magmas and the compositional gap at Sumisu submarine caldera, Izu–Bonin arc, Japan: Journal

- of Volcanology and Geothermal Research, v. 156, no. 3–4, p. 187–216. doi:10.1016/j.jvolgeores.2006.03.018
- Stacey, J.S., and Kramers, J., 1975, Approximation of terrestrial lead isotope evolution by a two-stage model: *Earth and Planetary Science Letters*, v. 26, no. 2, p. 207–221. doi:10.1016/0012-821X(75)90088-6
- Stern, R.J., Fouch, M.J., and Klempner, S., 2003, An overview of the Izu-Bonin-Mariana subduction factory, in Eiler, J., ed., *Inside the subduction factory*, Volume 138: Geophysical Monograph, Washington, D.C., American Geophysical Union, p. 175–222.
- Stern, R.J., and Scholl, D.W., 2010, Yin and yang of continental crust creation and destruction by plate tectonic processes: *International Geology Review*, v. 52, no. 1, p. 1–31. doi:10.1080/00206810903332322
- Suyehiro, K., Takahashi, N., Ariie, Y., Yokoi, Y., Hino, R., Shinohara, M., Kanazawa, T., Hirata, N., Tokuyama, H., and Taira, A., 1996, Continental crust, crustal underplating, and low-Q upper mantle beneath an oceanic island arc: *Science*, v. 272, no. 5260, p. 390–392. doi:10.1126/science.272.5260.390
- Tamura, Y., Busby, C., Blum, P., Guèrin, G., Andrews, G., Barker, A., Berger, J., Bongiolo, E., Bordiga, M., and DeBari, S., 2015, Expedition 350 summary, in *Proceedings of the International Ocean Discovery Program*, Volume 350: International Ocean Discovery Program, College Station, TX, p. 1–65.
- Tamura, Y., Gill, J.B., Tollstrup, D., Kawabata, H., Shukuno, H., Chang, Q., Miyazaki, T., Takahashi, T., Hirahara, Y., Kodaira, S., Ishizuka, O., Suzuki, T., Kido, Y., Fiske, R.S., and Tatsumi, Y., 2009, Silicic magmas in the Izu–Bonin oceanic arc and implications for crustal evolution: *Journal of Petrology*, v. 50, no. 4, p. 685–723. doi:10.1093/petrology/egp017
- Tamura, Y., Tani, K., Chang, Q., Shukuno, H., Kawabata, H., Ishizuka, O., and Fiske, R., 2007, Wet and dry basalt magma evolution at Torishima Volcano, Izu–Bonin Arc, Japan: The possible role of phengite in the downgoing slab: *Journal of Petrology*, v. 48, no. 10, p. 1999–2031. doi:10.1093/petrology/egm048
- Tamura, Y., Tani, K., Ishizuka, O., Chang, Q., Shukuno, H., and Fiske, R., 2005, Are arc basalts dry, wet, or both? Evidence from the Sumisu caldera volcano, Izu–Bonin arc, Japan: *Journal of Petrology*, v. 46, no. 9, p. 1769–1803. doi:10.1093/petrology/egi033
- Tani, K., Dunkley, D.J., Chang, Q., Nichols, A.R., Shukuno, H., Hirahara, Y., Ishizuka, O., Arima, M., and Tatsumi, Y., 2015, Pliocene granodioritic knoll with continental crust affinities discovered in the intra-oceanic Izu–Bonin–Mariana Arc: Syntectonic granitic crust formation during back-arc rifting: *Earth and Planetary Science Letters*, v. 424, p. 84–94. doi:10.1016/j.epsl.2015.05.019
- Tatsumi, Y., 2005, The subduction factory: How it operates in the evolving earth: *GSA Today*, v. 15, no. 7, p. 4. doi:10.1130/1052-5173(2005)015[4:TSFHIO]2.0.CO;2
- Taylor, B., 1992, Rifting and the volcanic-tectonic evolution of the Izu-Bonin-Mariana arc, in *Proceedings of the Ocean Drilling Program, Scientific Results*, Volume 126: College Station, TX, Ocean Drilling Program, p. 627–651.
- Taylor, R.N., and Nesbitt, R.W., 1998, Isotopic characteristics of subduction fluids in an intra-oceanic setting, Izu–Bonin Arc, Japan: *Earth and Planetary Science Letters*, v. 164, no. 1–2, p. 79–98. doi:10.1016/S0012-821X(98)00182-4
- Tollstrup, D., Gill, J., Kent, A., Prinkey, D., Williams, R., Tamura, Y., and Ishizuka, O., 2010, Across-arc geochemical trends in the Izu-Bonin arc: Contributions from the subducting slab, revisited: *Geochemistry, Geophysics, Geosystems*, 11, no. 1. doi:10.1029/2009GC002847
- Trail, D., Mojzsis, S.J., Harrison, T.M., Schmitt, A.K., Watson, E.B., and Young, E.D., 2007, Constraints on Hadean zircon protoliths from oxygen isotopes, Ti-thermometry, and rare earth elements: *Geochemistry, Geophysics, Geosystems*, 8, no. 6. doi:10.1029/2006GC001449
- Valley, J.W., 2003, Oxygen isotopes in zircon: *Reviews in Mineralogy and Geochemistry*, v. 53, no. 1, p. 343–385. doi:10.2113/0530343
- Vervoort, J.D., Patchett, P.J., Söderlund, U., and Baker, M., 2004, Isotopic composition of Yb and the determination of Lu concentrations and Lu/Hf ratios by isotope dilution using MC-ICPMS: *Geochim Geophys Geosyst*, v. 5. doi:10.1029/2004GC000721
- Wanless, V., Perfit, M., Ridley, W., and Klein, E., 2010, Dacite petrogenesis on mid-ocean ridges: Evidence for oceanic crustal melting and assimilation: *Journal of Petrology*, v. 51, no. 12, p. 2377–2410. doi:10.1093/petrology/egq056
- Wendt, I., and Carl, C., 1985, U/Pb dating of discordant 0.1 Ma old secondary U minerals: *Earth and Planetary Science Letters*, v. 73, no. 2–4, p. 278–284. doi:10.1016/0012-821X(85)90076-7
- Wiedenbeck, M., Allé, P., Corfu, F., Griffin, W., Meier, M., Oberli, F., Quadt, A.V., Roddick, J., and Spiegel, W., 1995, Three natural zircon standards for U-Th-Pb, Lu-Hf, trace element and REE analyses: *Geostandards and Geoanalytical Research*, v. 19, no. 1, p. 1–23. doi:10.1111/ggr.1995.19.issue-1
- Wiedenbeck, M., Hanchar, J.M., Peck, W.H., Sylvester, P., Valley, J., Whitehouse, M., Kronz, A., Morishita, Y., Nasdala, L., and Fiebig, J., 2004, Further characterisation of the 91500 zircon crystal: *Geostandards and Geoanalytical Research*, v. 28, no. 1, p. 9–39. doi:10.1111/j.1751-908X.2004.tb01041.x
- Williams, I., 1989, U-Th-Pb geochronology by ion microprobe, in McKibben, M., Shanks, W.I., and Ridley, W., eds., *Applications of microanalytical techniques to understanding mineralizing processes*: Littleton, CO, Society of Economic Geologists, p. 1–35.
- Woodhead, J., Hergt, J., Shelley, M., Eggins, S., and Kemp, R., 2004, Zircon Hf-isotope analysis with an excimer laser, depth profiling, ablation of complex geometries, and concomitant age estimation: *Chemical Geology*, v. 209, p. 121–135. doi:10.1016/j.chemgeo.2004.04.026
- Yokoyama, T., Kobayashi, K., Kuritani, T., and Nakamura, E., 2003, Mantle metasomatism and rapid ascent of slab components beneath island arcs: Evidence from  $^{238}\text{U}$ - $^{230}\text{Th}$ - $^{226}\text{Ra}$  disequilibria of Miyakejima volcano, Izu arc, Japan: *Journal of Geophysical Research: Solid Earth*, 108, no. B7. doi:10.1029/2002JB002103